Electronic Supplementary Information

for

Synthesis of substituent-free dioxadiaza[8]circulene to investigate intermolecular interactions and photophysical properties

Aoi Nakagawa,[a] Wataru Ota,[b] Takumi Ehara,[c] Yusuke Matsuo,[a] Kiyoshi Miyata,[c] Ken Onda,[c] Tohru Sato,*[a,d] Shu Seki*[a] and Takayuki Tanaka*[a]

[a]*Department of Molecular Engineering, Graduate School of Engineering, Kyoto University, Nishikyo-ku, Kyoto 615-8510, Japan*

[b]*MOLFEX, Inc., 34-4 Takano Nishibiraki-cho, Sakyo-ku, Kyoto 606-8103, Japan*

[c]*Department of Chemistry, Faculty of Science, Kyushu University, 744 Motooka, Nishi-ku, Fukuoka 819-0395, Japan*

[d]*Fukui Institute for Fundamental Chemistry, Kyoto University, 34-4 Takano Nishibiraki-cho, Sakyo-ku, Kyoto 606-8103, Japan*

*Email: tanaka@moleng.kyoto-u.ac.jp

Contents

1. Instrumentation and Materials

General information

Commercially available solvents and reagents were used without further purification unless otherwise noted. Dry THF was obtained by passing through alumina under N_2 in a solvent purification system. The spectroscopic grade solvents were used as solvents for all spectroscopic studies. Silica gel column chromatography was performed on Wako gel C-400 or C-300. Thin-layer chromatography (TLC) was carried out on aluminum sheets coated with silica gel 60 F_{254} (Merck 5554).

^1H and ^{13}C NMR spectra were recorded on a JEOL ECA-600 spectrometer (operating as 600 MHz for ^1H and 151 MHz for ^{13}C) or on a JEOL JNM-AL 400 MHz FT-NMR spectrometer (operating as 400 MHz for ^1H and 101 MHz for ^{13}C) and chemical shifts were reported as the δ scale in ppm relative to internal standards $CHCl_3$ (δ = 7.26 ppm for ^1H, 77.16 ppm for ^{13}C), DMSO (δ = 2.50 ppm for ^1H, 39.52 ppm for ^{13}C), and acetone-d_6 (δ = 2.05 ppm for ^1H). HR-APCI-TOF-MS and HR-ESI-TOF-MS were recorded on a BRUKER micrOTOF model or ultrafleXtreme model or Thermo Fisher Scientific LTQ orbitrap XL model using positive mode.

UV-Visible absorption spectra were recorded on a Shimadzu UV-3600. Fluorescence spectra were recorded on a JASCO FP-8500 spectrometer. Absolute fluorescence quantum yields were determined on a HAMAMATSU C9920-02S. Fluorescence lifetime was recorded on a Hamamatsu Photonics Quantaurus-Tau C11367. Thermogravimetric analysis (TGA) was performed in nitrogen gas using a Shimadzu TGA-50 equipped with an aluminum pan and heated at a rate of 5 °C per minute.

Time-resolved photoluminescence spectroscopy (TR-PL) measurements were performed using a polychromator and a streak camera system (Hamamatsu C4780) with a time resolution of less than 30 ps. The light source for optical excitation was a Ti:sapphire regenerative amplifier (Spectra-Physics, Spitfire Ace, pulse duration: 120 fs, repetition rate: 1 kHz, pulse energy: 3.6 mJ/pulse, and central wavelength: 800 nm) seeded by a Ti:sapphire femtosecond mode-locked laser (Spectra-Physics, Tsunami). The excitation light (wavelength = 350 nm, fluence at sample position = 1.3 mJ/cm^2) was generated using fourth harmonic generation of the signal light (1400 nm) from an optical parametric amplifier (Light conversion, TOPAS) pumped by the amplifier.

Single-crystal diffraction analysis data were collected at –180 °C with a Rigaku XtaLAB P200 by using graphite monochromated Cu-$K\alpha$ radiation (λ = 1.54187 Å) or with a Rigaku Saturn724+ CCD diffractometer with a graphite-monochromated Mo Kα radiation (λ = 0.71073 Å). The structures were solved by direct methods (SHELXT-2014/5) and refined with full-matrix least squares technique (SHELXT-2014/7).[S1]

Redox potentials were measured on an ALS electrochemical analyzer model 612E by cyclic voltammetry (CV) and differential pulse voltammetry (DPV).

All calculations were carried out using the Gaussian 16 program.[S2] All structures were fully optimized without any symmetry restriction. The calculations were performed by the DFT method with restricted B3LYP/6-311G(d,p) level[S3] for all atoms. NICS values were obtained with the GIAO method at the B3LYP/6-311G(d,p) level.[S4] Excitation energies and oscillator strengths were calculated with the TD-SCF method at the B3LYP/6-311G(d,p) level. The vibronic coupling constants (VCCs) and fluorescence spectrum were computed using our in-house codes.

2. Experimental Section

3,6-Dibromocarbazole

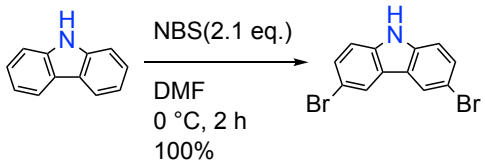

Carbazole (25.6 g, 153 mmol) was dissolved in DMF (100 mL), and a solution of NBS (60.9 g, 0.342 mmol) in DMF (200 mL) was added dropwise and the mixture was stirred at 0 °C for 2 h. Water (1500 mL) was added and the solid of 3,6-dibromocarbazole was obtained by filtration and dried under vacuum. Yield: 49.9 g (153 mmol), 100%. TLC: R_f = 0.34 (ethyl acetate / *n*-hexane, 1:4); ^{1}H NMR (600 MHz, $CDCl_3$): δ =8.17 (br, 1H), 8.13 (d, J = 1.4 Hz, 2H), 7.52 (dd, J = 8.7, 1.4 Hz, 2H) and 7.32 (d, J = 8.7 Hz, 2H) ppm. The data are in consistent with the reported ones except for the chemical shifts of NH.[S5]

3,6-Dibromo-*N*-(2-phenylethyl)carbazole (7)

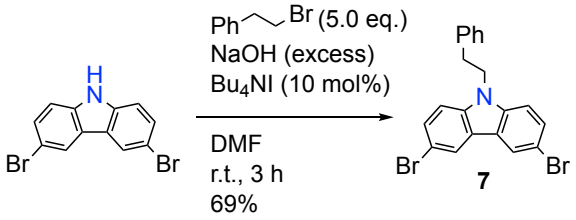

3,6-Dibromocarbazole (49.9 g, 153 mmol) was dissolved in DMF (200 mL), and well crushed NaOH (100 g, 2.5 mol) was added. After 10 min stirring, Bu_4NI (5.5 g, 15 mmol) and 2-bromoethylbenzene (100 mL, 750 mmol) were added and the mixture was stirred at room temperature for 3 h. After water (1000 mL) was added, the organic phase was extracted three times with toluene, washed with water and saturated brine, dried over anhydrous Na_2SO_4, and concentrated under reduced pressure. White solid of **7** was recrystallized from methanol. Yield: 45.5 g (106 mmol), 69%. TLC: R_f = 0.34 (ethyl acetate/*n*-hexane, 1:4); ^{1}H NMR (600 MHz, $CDCl_3$): δ =8.13 (d, J = 2.3 Hz, 2H), 7.49 (dd, 8.5, 2.1 Hz, 2H), 7.18-7.28 (m,3H), 7.12 (d, J = 8.3 Hz, 2H), 7.05 (dd, J = 7.6, 1.6 Hz, 2H), 4.47 (t, J = 7.3 Hz), and 3.09 (t, J = 7.3 Hz, 2H) ppm; ^{13}C NMR (100 MHz, $CDCl_3$): δ = 139.12, 138.16, 129.00, 128.70, 123.46, 122.09, 45.16 and 35.11 ppm. HR-APCI-MS (positive): found *m/z* = 427.9642 (calcd for $C_{20}H_{16}NBr^{79}_2$ = 427.9644 $[M+H]^+$)

3,6-Dimethoxy-*N*-(2-phenylethyl)carbazole (8)

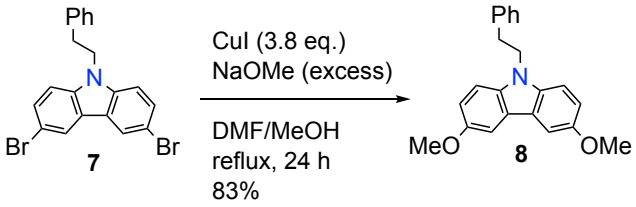

7 and copper(I) iodide (75 g, 400 mmol) were suspended in DMF (300 mL), to which sodium methoxide (131 g, 2.42 mol) methanol (500 ml) solution was added. The mixture was stirred at reflux for 24 h. The reaction was quenched by adding water (4000 mL), and the resulting precipitate was filtered. The obtained solid was dissolved in acetone and filtered again to remove insoluble solids. The solvent was removed under reduced pressure, and the crude product was dissolved in dichloromethane (500 ml). The solution was washed four times with 25% aqueous ammonia solution, water, and saturated brine, dried over Na_2SO_4, and concentrated under reduced pressure. White acicular crystals of **8** was obtained by recrystallization from methanol. Yield: 29.1 g, 83%. TLC: R_f = 0.36(EtOAc/hexane, 1:4); ^{1}H NMR (600 MHz, acetone-d_6):δ = 3.10 (t, J = 7.6 Hz, 2H), 3.88 (s, 6H), 4.56 (t, J = 7.6 Hz, 2H,), 7.02 (dd, J = 8.9, 2.5 Hz, 2H), 7.17 (m,1H), 7.23 (m, 4H), 7.37 (d, J = 9.2 Hz, 2H), 7.67- ppm (d, J = 2.3 Hz, 2H); ^{13}C NMR (400 MHz, $CDCl_3$):δ = 35.36, 45.13, 56.11, 103.11, 109.36, 114.96, 122.86, 126.56, 128.59, 128.74, 135.82, 138.80, 153.24 ppm. HR-APCI-MS (positive): found m/z = 322.1645 (calcd for $C_{22}H_{22}N_1O_2$ = 322.1645 $[M+H]^+$)

2,7-Di-*tert*-butyl-3,6-dimethoxy-*N*-(2-phenylethyl)carbazole (9)

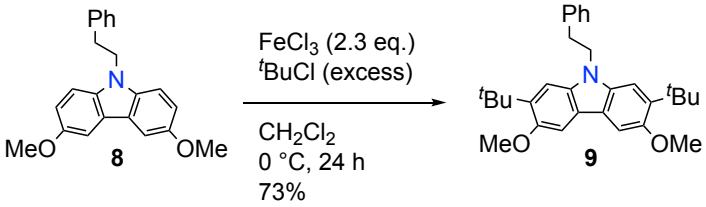

To the suspension of **8** (10.8 g, 33 mmol) and iron(III) chloride (4.08 g, 25 mmol) in dry dichloromethane (150 mL) cooled to 0 °C under nitrogen atmosphere was added 2-chloro-2-methylpropane (200 mL, 900 mmol) dropwise over 1 h. After the mixture was stirred overnight at 0 °C, iron(III) chloride (4.27 g, 26 mmol) was added and the mixture was stirred for 2.5 h. Another iron(III) chloride (4.10 g, 25 mmol) was added and the mixture was further stirred for 3 h. The reaction mixture was quenched with HCl (3 M, 300 mL), and the aqueous phase was extracted twice with dichloromethane. The combined organic phase was washed with water three times and saturated brine once, dried over anhydrous Na_2SO_4 and concentrated under reduced pressure. A white solid of **9** was recrystallized from methanol. Yield: 10.6 g (24 mmol), 73%. TLC: R_f = 0.71 (ethyl acetate / *n*-hexane, 1:4); ^{1}H NMR (600 MHz, $CDCl_3$): δ = 7.44 (s, 2H), 7.17-7.22 (m,3H), 7.08 (m, 4H), 4.46 (t, J = 7.1 Hz, 2H), 3.96 (s, 6H), 3.07 (t, J = 7.1 Hz, 2H) and 1.44 (s, 18H) ppm; ^{13}C NMR (100 MHz, $CDCl_3$):

δ = 152.72, 137.14, 135.22, 128.90, 128.54, 126.45, 120.21, 102.46, 55.80, 44.79, 35.73, 35.42 and 30.09 ppm. HR-APCI-MS (positive): found *m/z* = 444.2893 (calcd for $C_{30}H_{38}N_1O_2$ = 444.2897 $[M+H]^+$)

2,7-Di-*tert*-butyl-3,6-hydroxy-*N*-(2-phenylethyl)carbazole (8)

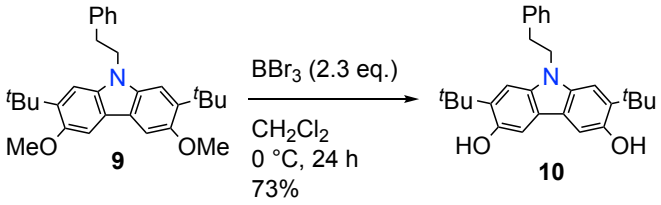

To the solution of **9** (4.92 g, 11 mmol) in dichloromethane (20 mL) under nitrogen atmosphere was added BBr_3 (1 M dichloromethane solution, 25 mL) dropwise at 0 °C. Another dichloromethane (20 mL) was added, and the mixture was stirred overnight. After further stirring at room temperature for 3 h, HCl (1 M, 100 mL) was added, and the aqueous phase was extracted with dichloromethane twice. The combined organic phase was dried over anhydrous Na_2SO_4 and concentrated under reduced pressure. The crude product was purified by using column chromatography (ethyl acetate / *n*-hexane, 1:4) to yield a pure white powder of **10**. Yield: 3.36 g (8.1 mmol), 73%. TLC: R_f = 0.25 (ethyl acetate / *n*-hexane, 1:4); ^{1}H NMR (600 MHz, $CDCl_3$): δ = 7,15-7.21 (m, 5H), 7.05 (m, 4H), 4.56 (br, 2H), 4.45 (t, J = 7.1 Hz, 2H), 3.07 (t, J = 7.1 Hz, 2H) and 1.47 (s, 18H) ppm; ^{13}C NMR (100 MHz, $CDCl_3$):δ = 147.43, 139.22, 135.80, 128.47, 126.38, 119.87, 106.64, 44.82, 35.52, 35.20 and 29.83 ppm. HR-APCI-MS (positive): found *m/z* = 416.2580 (calcd for $C_{28}H_{34}N_1O_2$ = 416.2584 $[M+H]^+$)

N,N'-(2-phenethyl)-tetra-*tert*-butyldioxadiaza[8]circulene (6-PE-^{t}Bu)

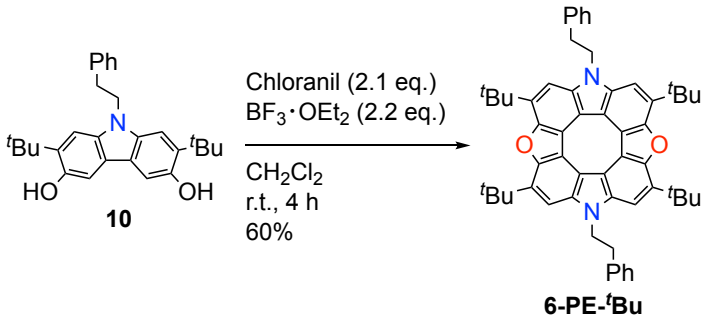

To the mixture of **10** (3.02 g, 7.2 mmol) and 2,3,5,6-tetrachloro-1,4-benzoquinone (chloranil, 930 mg, 3.8 mmol) in dry dichloromethane (300 mL) under nitrogen atmosphere was added boron trifluoride diethyl ether complex ($BF_3 \cdot OEt_2$, 1.0 mL, 8.0 mmol). Chloranil (930 mg, 3.8 mmol) was added for each time after stirring for 45 min, 1.5 h and 3.5 h and $BF_3 \bullet OEt_2$ (1.0 mL, 8.0 mmol) was added after 1.5 h. The mixture was stirred for 4 h in total. HCl (1 M, 300 mL) was added, and the aqueous phase was extracted four times with dichloromethane. The combined organic phase was dried over

anhydrous Na_2SO_4, and the solvent was removed under reduced pressure to give a black solid. The crude product was stirred at 120 °C overnight with potassium hydroxide (60 g, 720 mmol), toluene (250 mL) and ethanol (250 mL). HCl (2 M, 400 mL) was added, and the aqueous phase was extracted with dichloromethane four times. The combined organic phase was dried over Na_2SO_4 and concentrated under reduced pressure. The residue was purified by column chromatography (THF / *n*-hexane, 3:1) to give a yellow solid of **6-PE-^{t}Bu**. Yield: 1.73 g (2.2 mmol), 60%. TLC: R_f = 0.70 (ethyl acetate / *n*-hexane, 1:4); ^{1}H NMR (600 MHz, $CDCl_3$): δ = 7.24 (s, 4H), 7.16 (m, 6H), 7.05 (m, 4H), 4.82 (t, J = 6.7 Hz, 4H), 3,27 (t, J = 6.9 Hz, 4H) and 1.73 (s, 36H) ppm; ^{13}C NMR (100 MHz, $CDCl_3$): δ = 149.37, 139.32, 136.49, 132.97, 129.01, 128.57, 126.50, 116.67, 112.42, 104.57, 45.64, 36.29, 35.01 and 30.44 ppm. HR-APCI-MS (positive): found *m/z* = 791.4552 (calcd for $C_{56}H_{59}N_2O_2$ = 791.4571 $[M+H]^+$)

Tetra-*tert*-butyldioxadiaza[8]circulene (6-^{t}Bu)

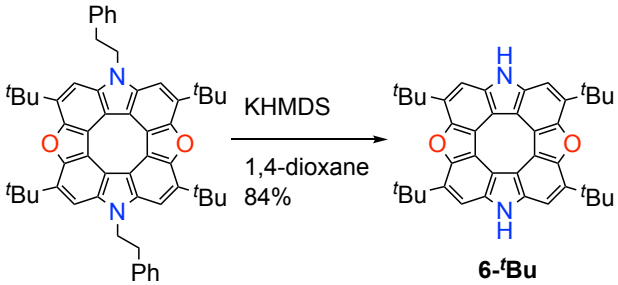

6-PE-^{t}Bu **6-^{t}Bu**

To the solution of **6-PE-^{t}Bu** (598 mg, 0.76 mmol) in 1,4-dioxane (300 mL) under nitrogen atmosphere was added potassium hexamethyldisilazide toluene solution (0.5 M, 45 mL, 23 mmol) and the mixture was stirred at 120 °C for 22 h. Then saturated aqueous ammonium chloride solution (400 mL) was added, and the aqueous phase was extracted three times with ethyl acetate. The combined organic phase was dried over anhydrous Na_2SO_4, and the solvent was removed under reduced pressure to precipitate a solid. The obtained solid was washed with dichloromethane several times to yield a white powder of **6-^{t}Bu**. Yield: 369 mg (0.63 mmol), 84%. TLC: R_f = 0.45 (ethyl acetate / *n*-hexane, 1:4); ^{1}H NMR (600 MHz, $CDCl_3$): δ = 8.37 (br, 2H), 7.56 (s, 4H) and 1.78 (s, 36H) ppm; ^{13}C NMR (100 MHz, $CDCl_3$): δ = 149.58, 135.98, 133.56, 116.66, 113.45, 106.46, 35.05 and 30.47 ppm. HR-APCI-MS (positive): found *m/z* = 583.3305 (calcd for $C_{40}H_{43}N_2O_2$ = 583.3319 $[M+H]^+$)

Dioxadiaza[8]circulene (6)

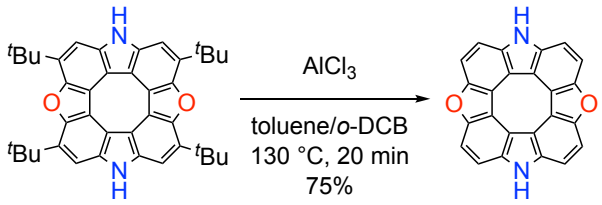

6-^{t}Bu **6**

To the solution of **6-^{t}Bu** (54.3 mg, 0.093 mmol) in toluene (50 mL) and *o*-dichlorobenzene (50 mL) under nitrogen atmosphere was added aluminium chloride (259 mg, 1.9 mmol). The mixture was stirred at 130 °C for 20 min and then cooled to room temperature. Yellow powder of **6** was obtained by column chromatography (toluene / THF (3:1)) followed by recrystallization from *n*-hexane. Yield: 25.1 mg (0.070 mmol), 75%. ^{1}H NMR (600 MHz, DMSO-d_6): δ = 11.93 (br, 2H), 7.92 (d, J = 8.7 Hz, 4H) and 7.82 (d, J = 8.7 Hz, 4H); ^{13}C NMR (100 MHz, DMSO-d_6): δ = 150.51, 136.23, 115.10, 113.32, 111.01 and 109.97 ppm. HR-APCI-MS (positive): found m/z = 359.0813 (calcd for $C_{24}H_{11}N_2O_2$ = 359.0813 $[M+H]^+$).

Solubility tests for hetero[8]circulenes 6-PE-^{t}Bu, 6-^{t}Bu

Table S1. *Comparison of the solubilities of* ***1-6*** *in THF, DMSO and CH_2Cl_2.*

	1[S6]	**2**[S7]	**3**[S8]	**4**[S9]	**5**[S10]	**6**
THF	○	○	×	○	×	○
DMSO	○	○	○	○	×	○
CH_2Cl_2	×	~0	×	*"poor"*	×	~0

For compound **2**, the solubilities in common organic solvents have been examined in our previous work,[S7] where the solubilities were measured by the following procedures.

(1) A small amount of solvents was added to the solids of **2**.

(2) The resulting suspension was sonicated for 30 sec and the insoluble residue was removed by filtration.

(3) The weight of the saturated solution (filtrate) was measured.

Table S2. *Reported solubilities of* **2** *in various organic solvents.*

	acetone	CH_2Cl_2	*n*-hexane	toluene	methanol	diethyl ether	THF

(mg/mL)	4.6	0.15	~0	~0	4.2	0.54	21

Using a similar method, we have roughly examined the solubilities of **6-PE-^{t}Bu**, **6-^{t}Bu** and **6**, the summary of which is shown in Table S3.

Table S3. *Solubilities of* ***6*** *in various organic solvents.*

	acetone	CH_2Cl_2	*n*-hexane	toluene	methanol	THF	DMSO
6-PE-^{t}Bu (mg/mL)	~0	17	~0	2.3	~0	18	~0
6-^{t}Bu (mg/mL)	~0	1.2	~0	1.0	0.5	10	0.4
6 (mg/mL)	0.4	~0	~0	~0	~0	2.2	2.0

Hear, "~0" means the solubility is less than 0.25 mg/mL (measurement lower limit). Compared with **2**, the solubility of **6** in organic solvents are rather poor, while **6-PE-^{t}Bu** and **6-^{t}Bu** are relatively soluble in toluene, THF and CH_2Cl_2.

3. NMR Spectra

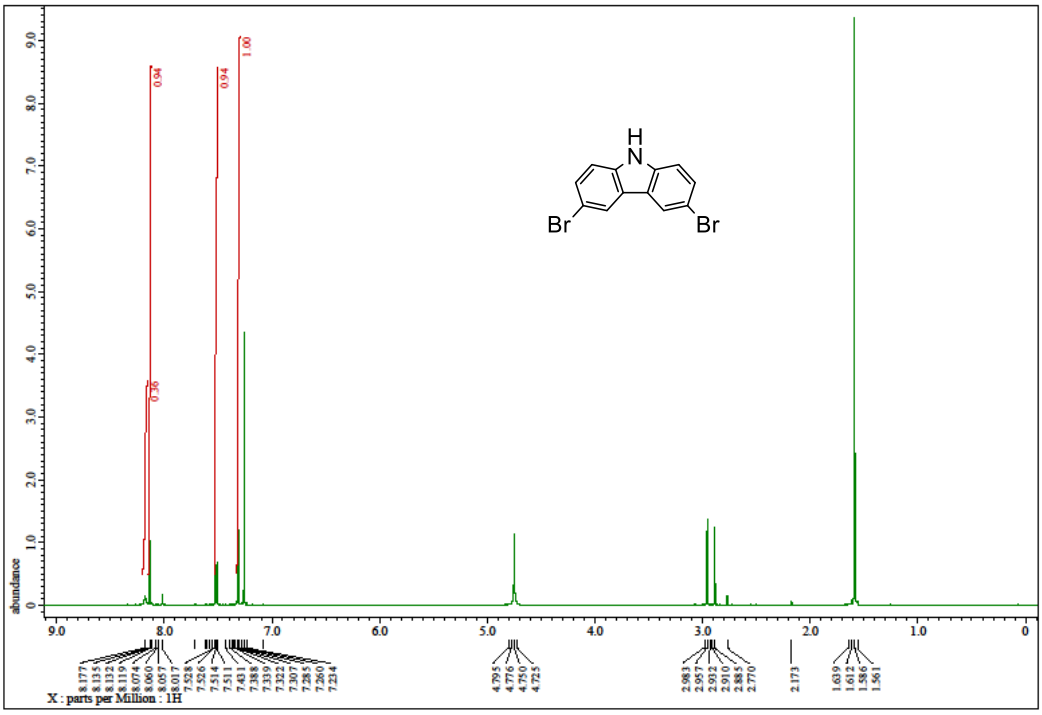

Fig. S3-1 ^{1}H NMR spectrum of 3,6-dibromocarbazole in $CDCl_3$.

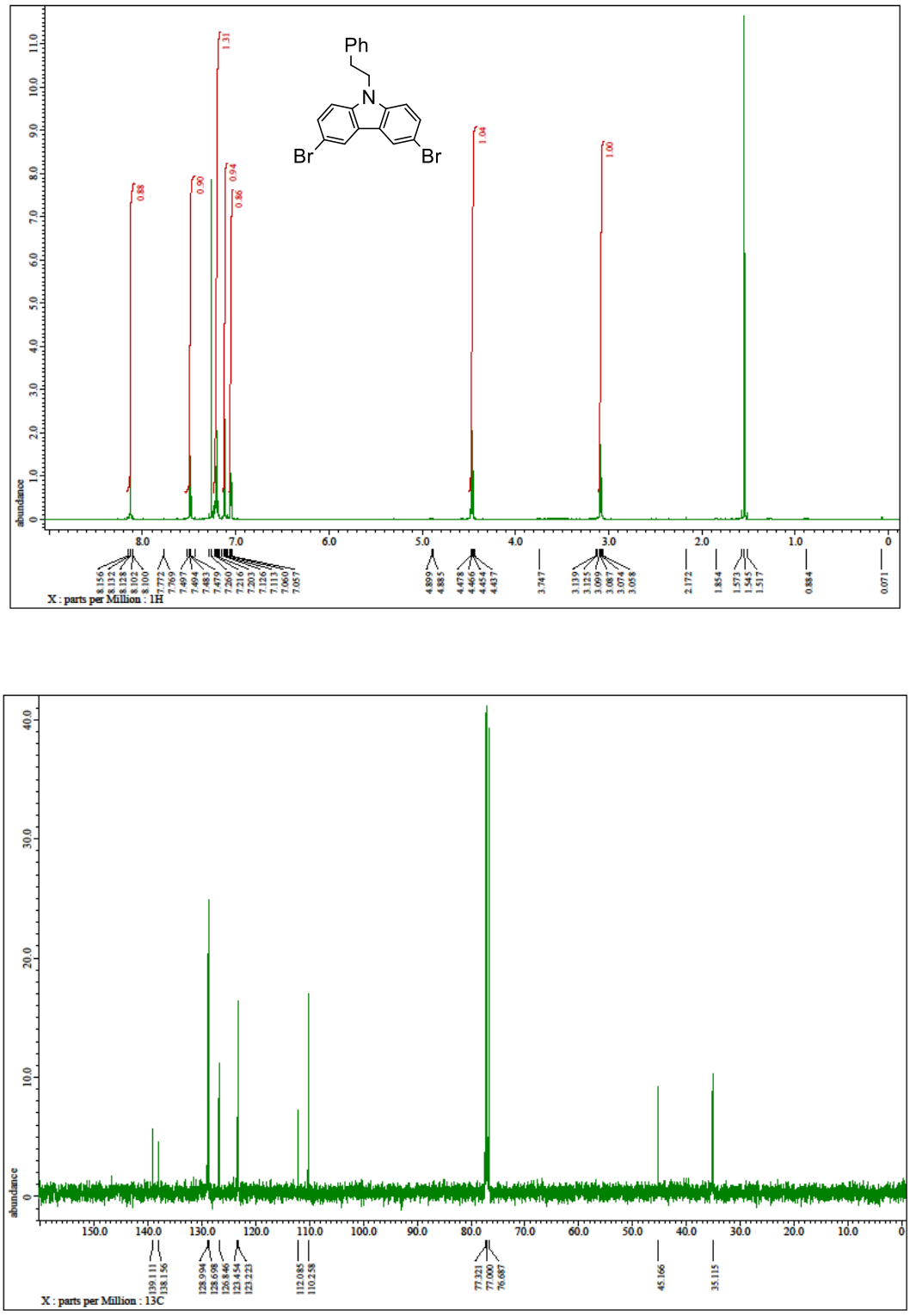

Fig. S3-2 ^{1}H and ^{13}C NMR spectra of 3,6-dibromo-*N*-(2-phenylethyl)carbazole in $CDCl_3$.

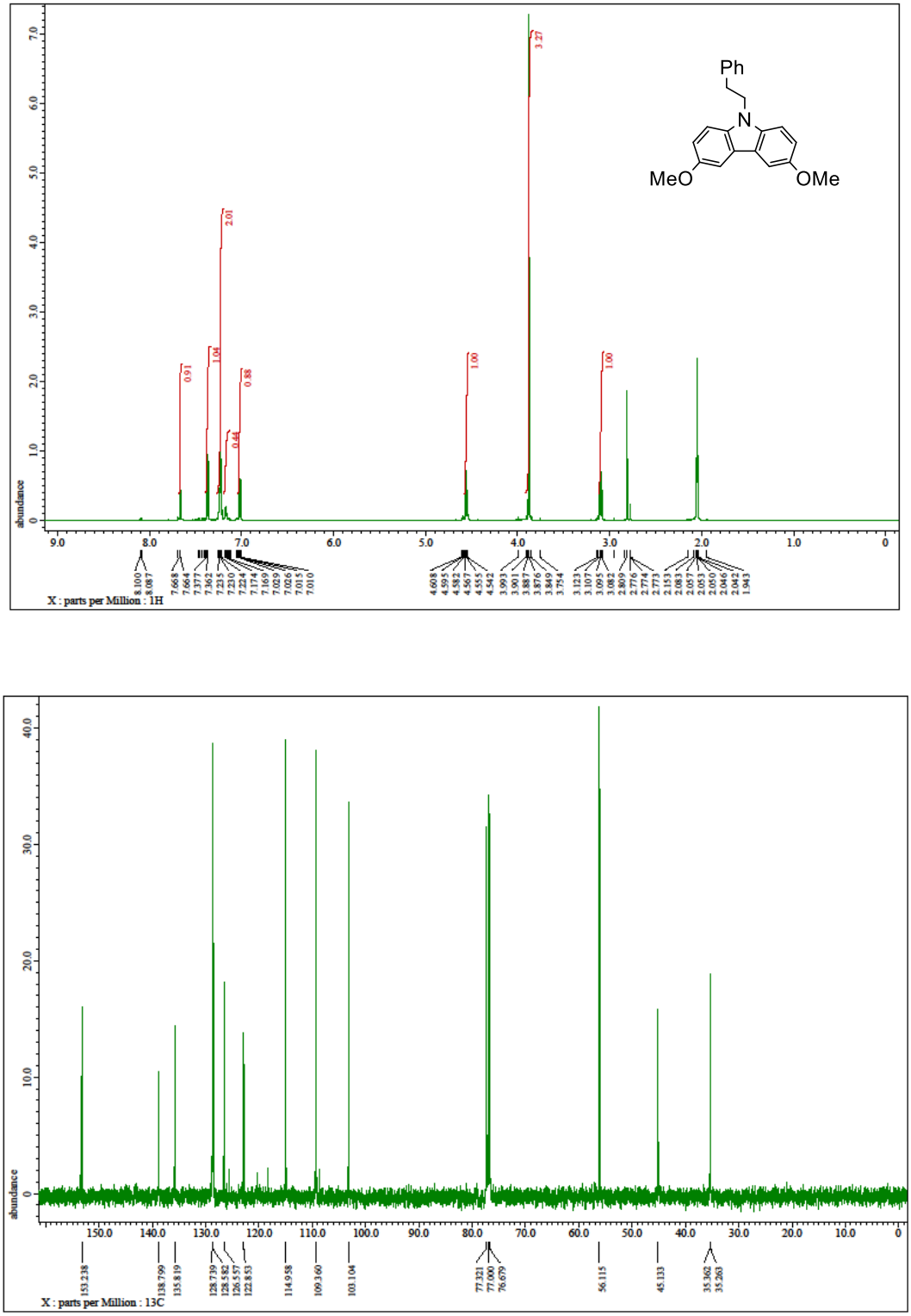

Fig. S3-3 ^{1}H and ^{13}C NMR spectra of **8** in acetone-d_6 for ^{1}H and in $CDCl_3$ for ^{13}C.

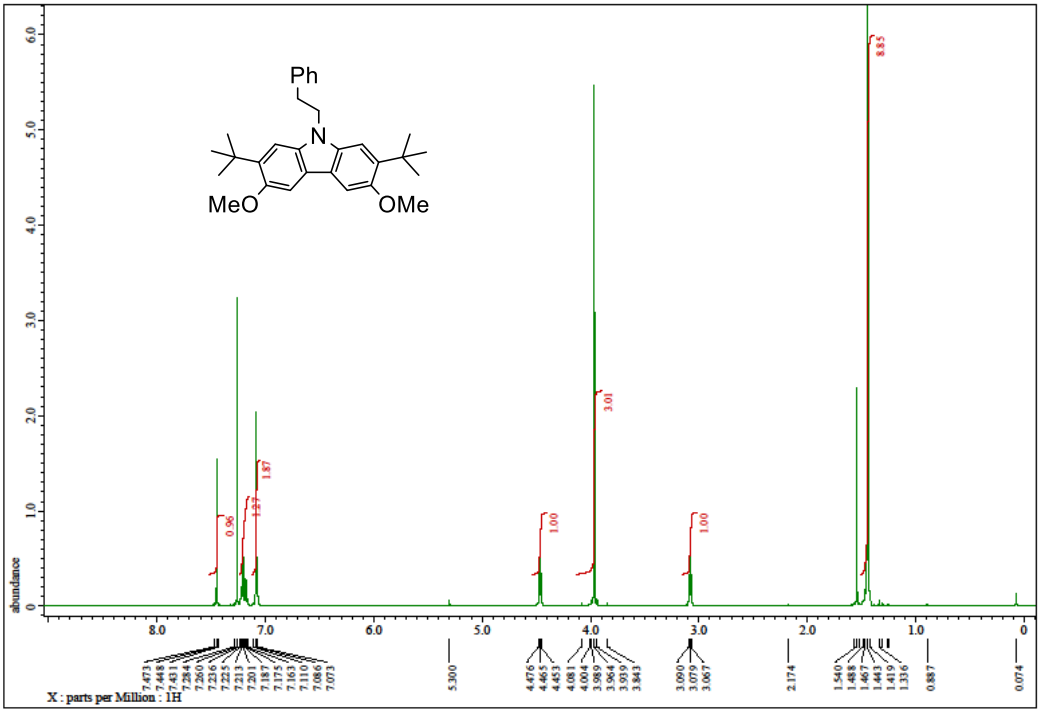

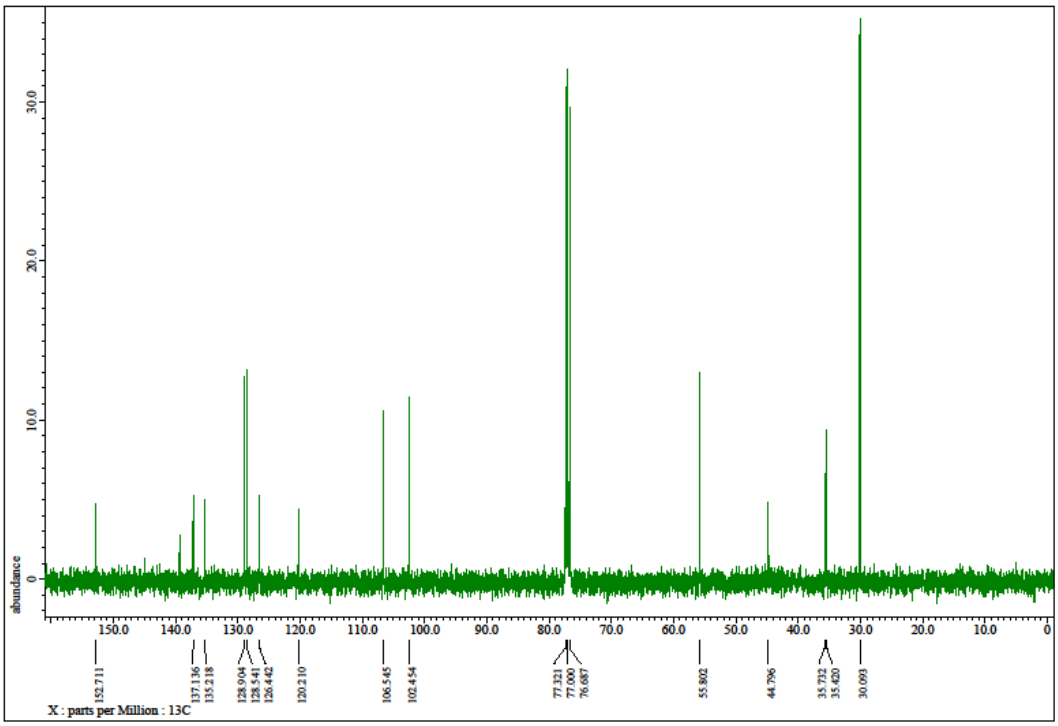

Fig. S3-4 ^{1}H and ^{13}C NMR spectra of **9** in $CDCl_3$.

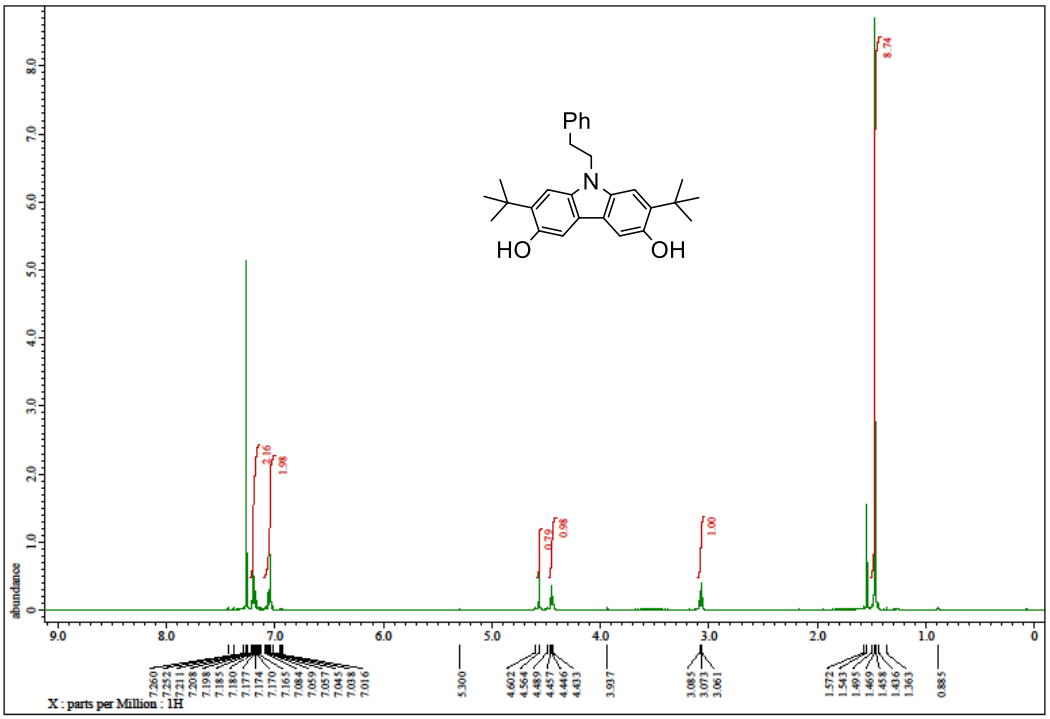

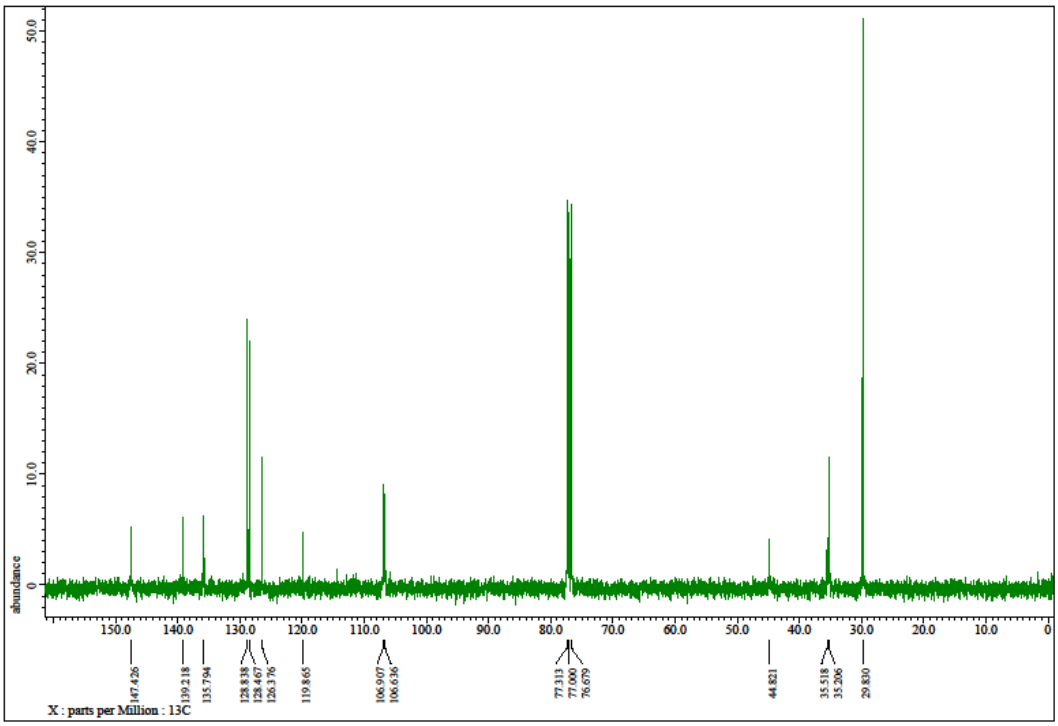

Fig. S3-5 ^{1}H and ^{13}C NMR spectra of **10** in $CDCl_3$.

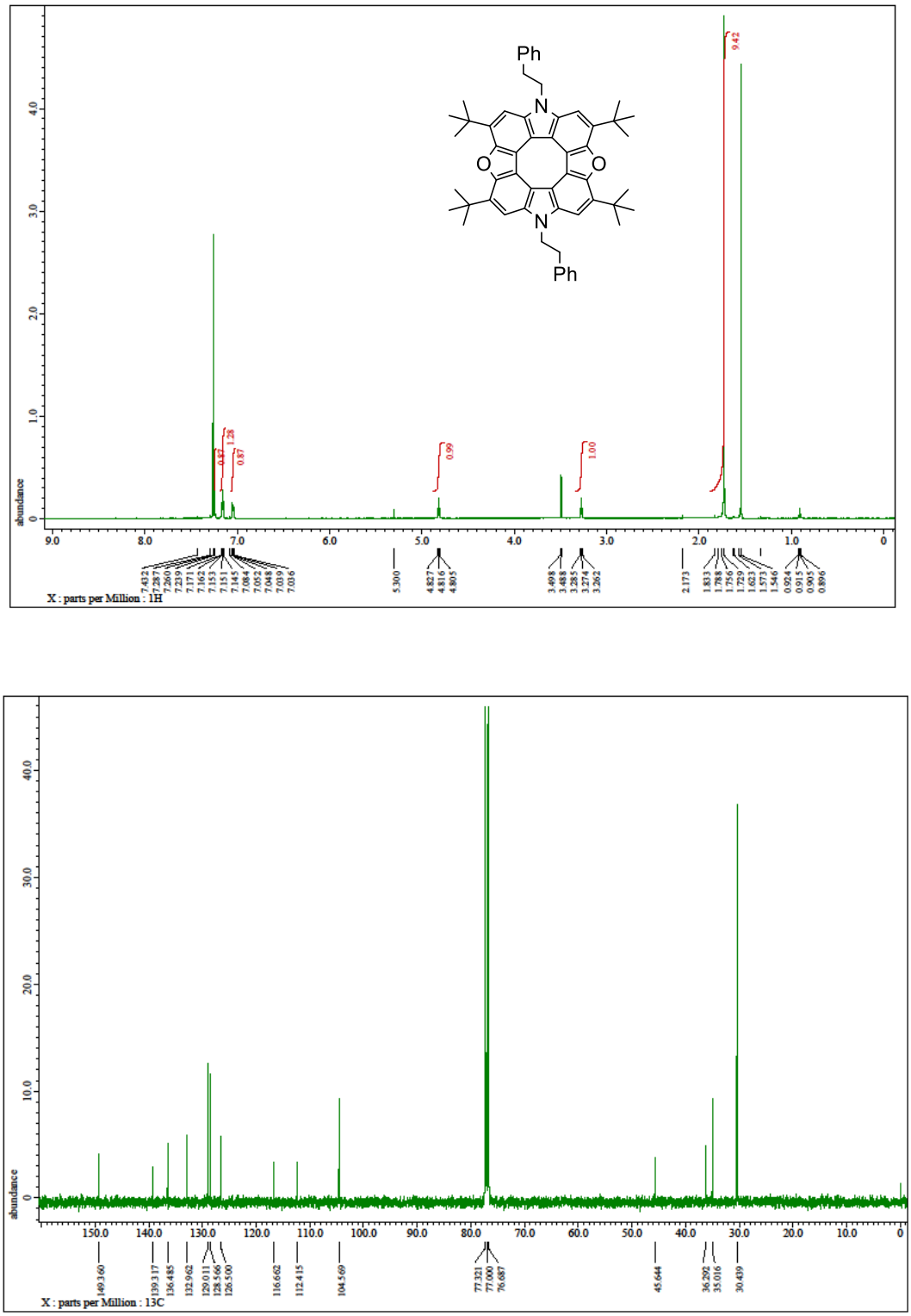

Fig. S3-6 ^{1}H and ^{13}C NMR spectra of **6-PE-^{t}Bu** in $CDCl_3$.

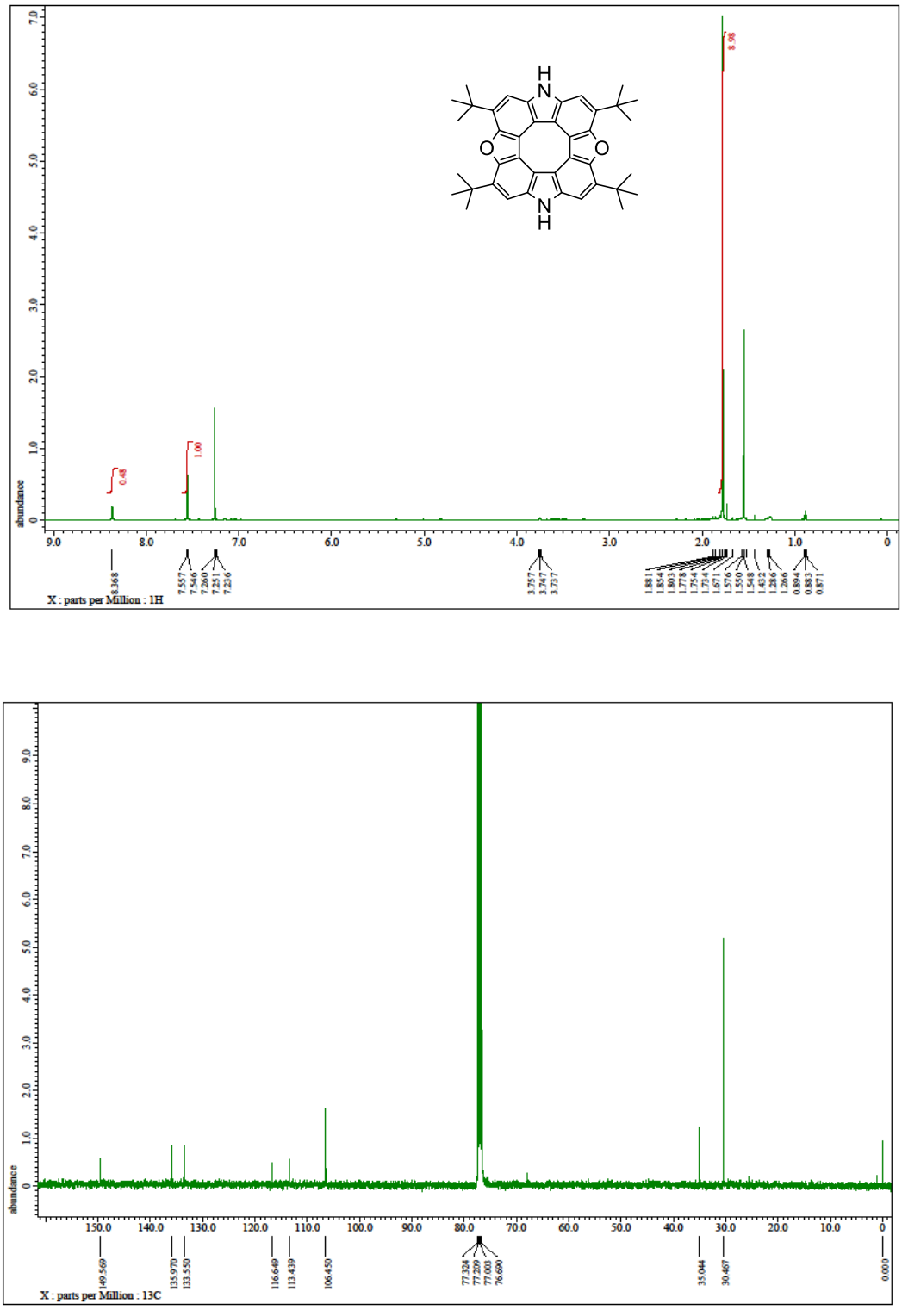

Fig. S3-7 ^{1}H and ^{13}C NMR spectra of **6-^{t}Bu** in $CDCl_3$.

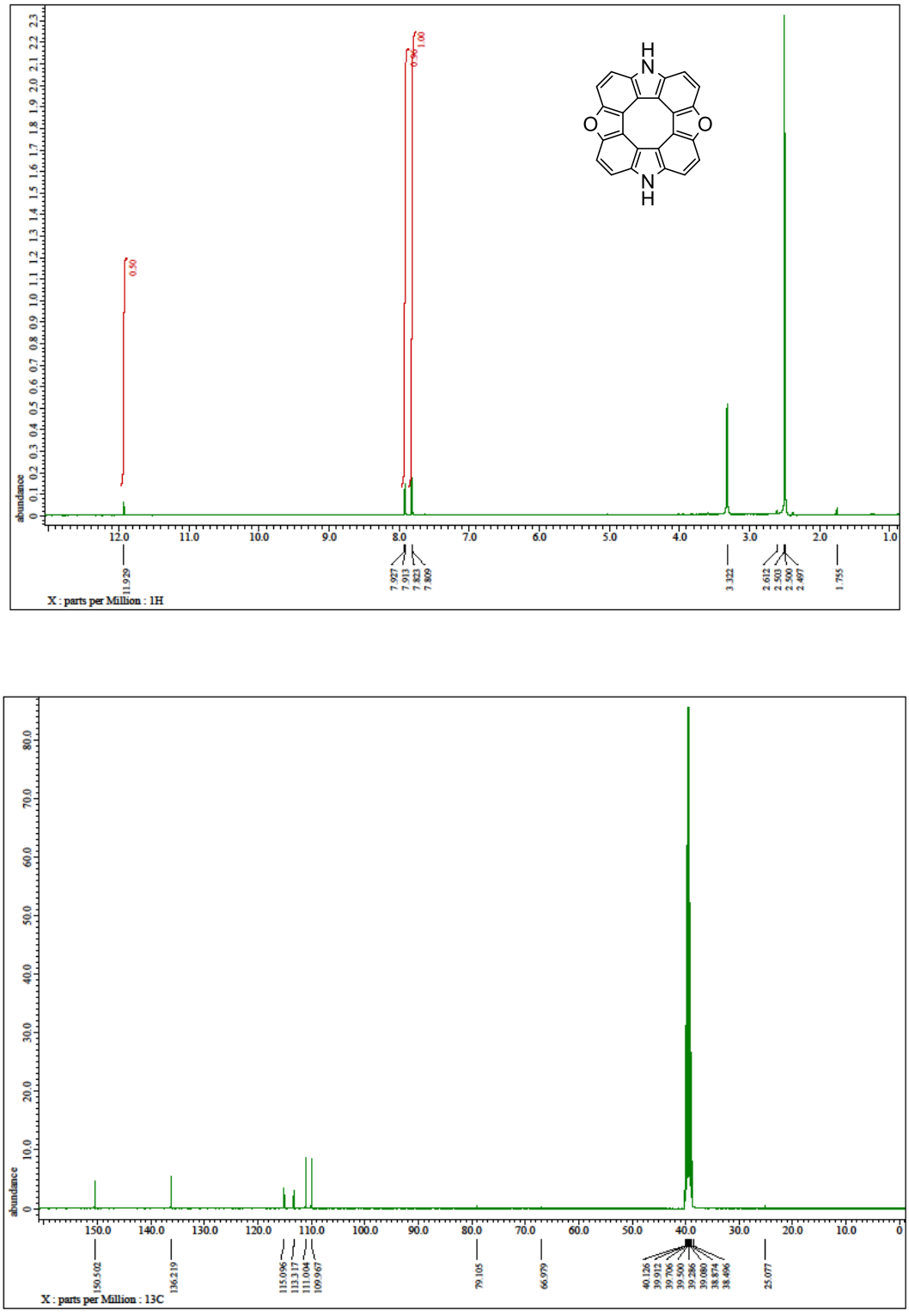

Fig. S3-8 ^{1}H and ^{13}C NMR spectra of **6** in DMSO-d_6.

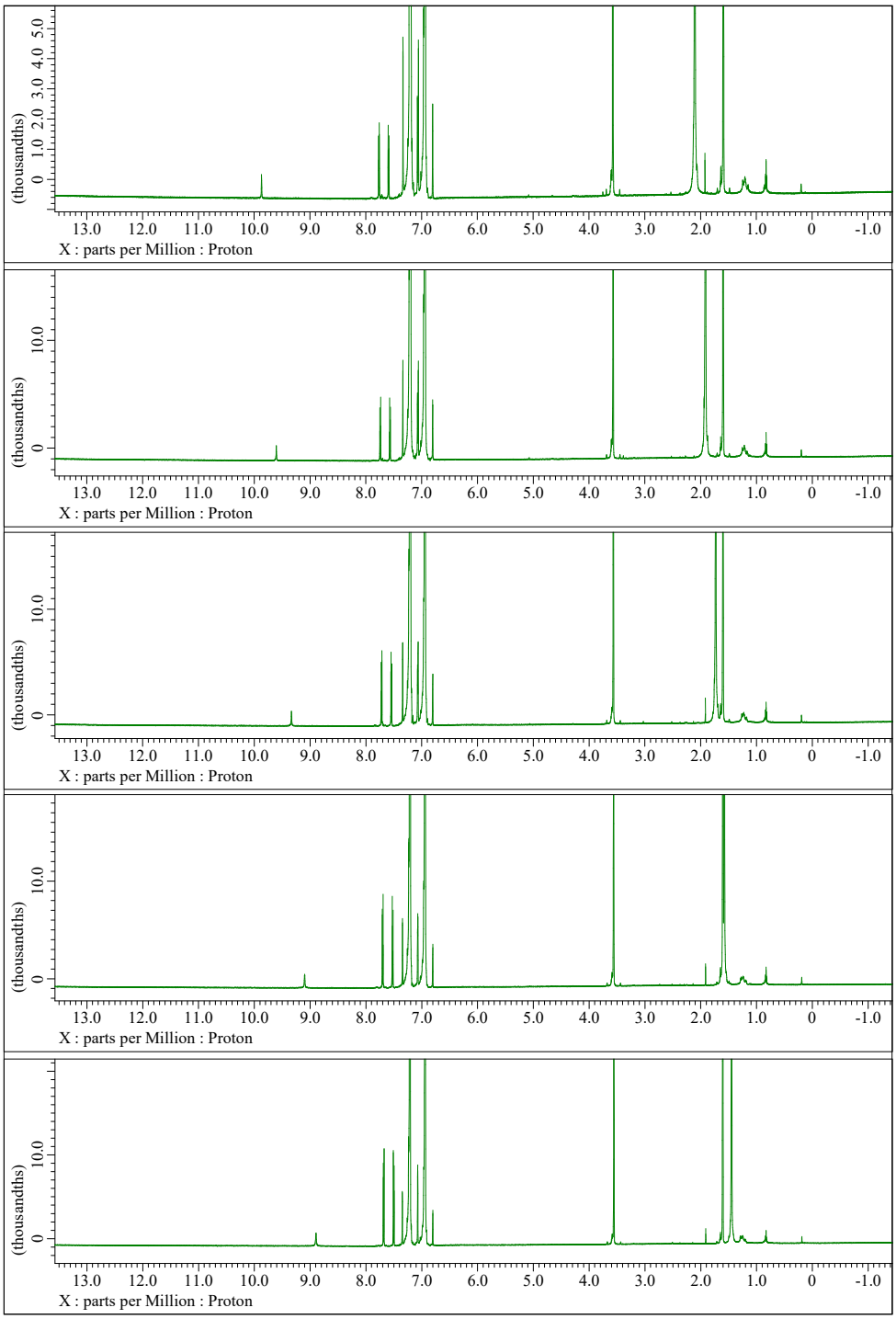

Fig. S3-9 Variable-temperature ^{1}H NMR spectra of **6** in the mixture of 1,2-dichlorobenzene-d_4 and THF-d_8 (v/v = 9/1). From top to bottom, room temperature, 313 K, 333 K, 353 K, and 373 K.

4. Mass Spectra

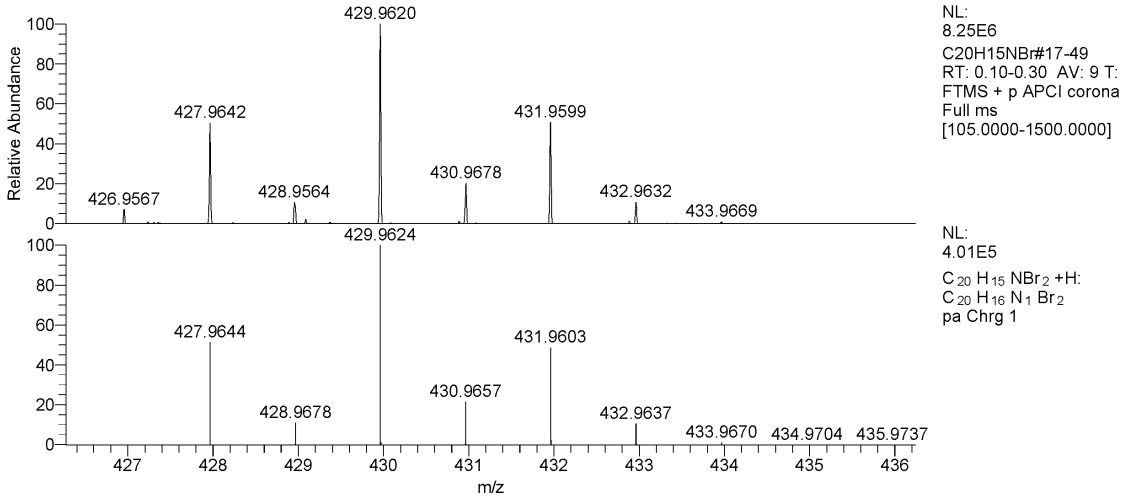

Fig. S4-1 APCI mass spectra of **7**. (Top: observed. Bottom: calculated for $[M+H]^+$.)

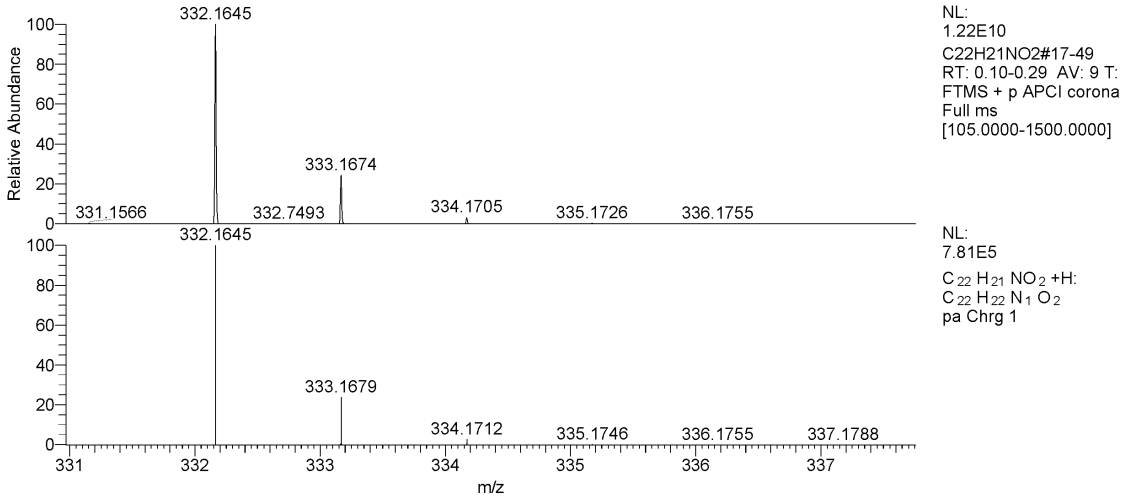

Fig. S4-2 APCI mass spectra of **8**. (Top: observed. Bottom: calculated for $[M+H]^+$.)

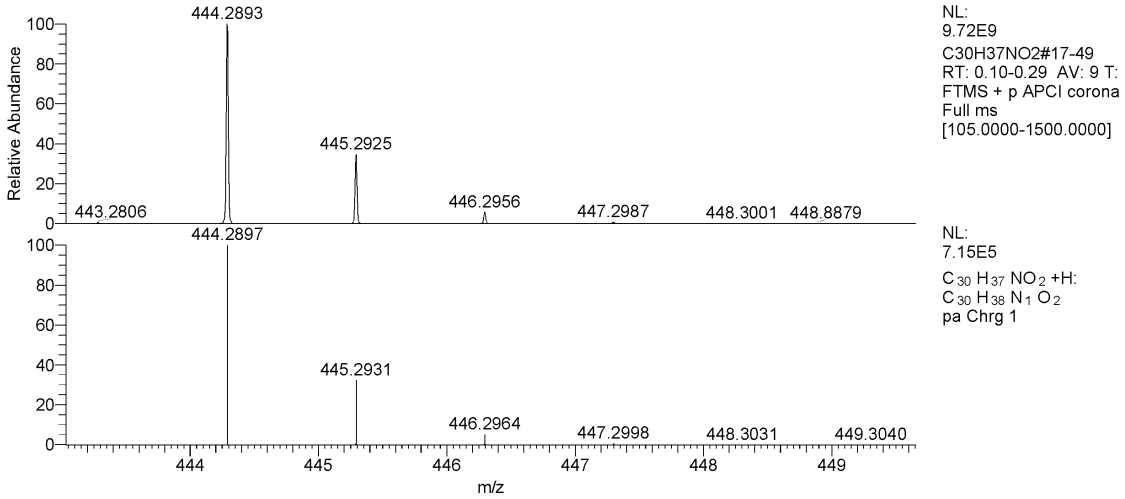

Fig. S4-3 APCI mass spectra of **9**. (Top: observed. Bottom: calculated for $[M+H]^+$.)

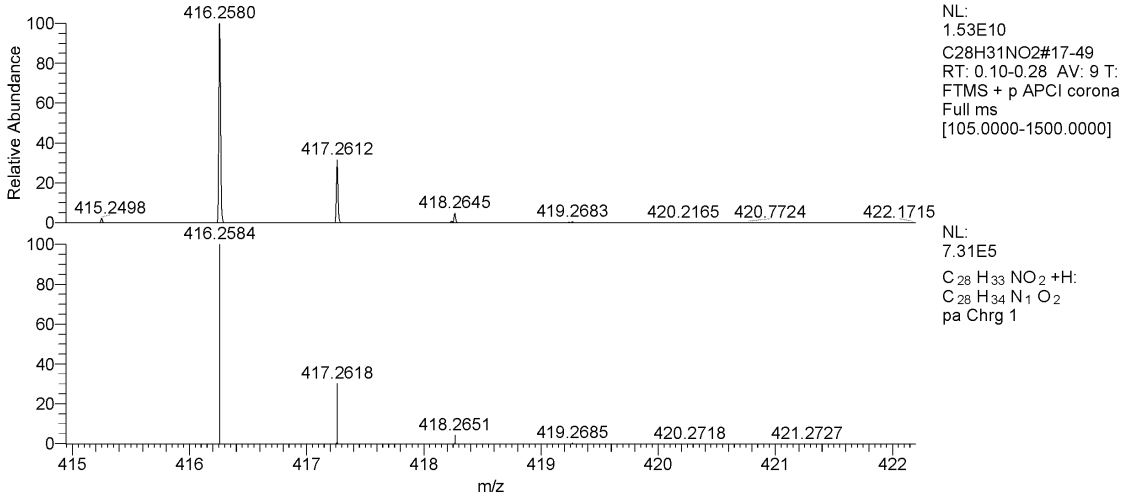

Fig. S4-4 APCI mass spectra of **10**. (Top: observed. Bottom: calculated for $[M+H]^+$.)

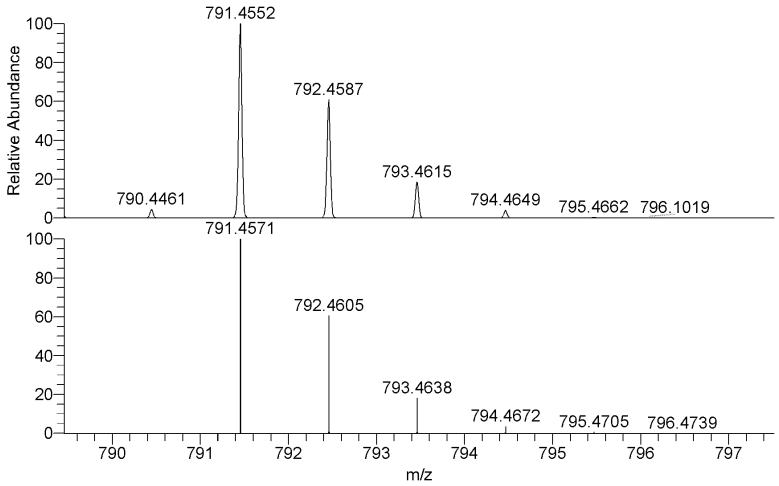

Fig. S4-5 APCI mass spectra of **6-PE-^{t}Bu**. (Top: observed. Bottom: calculated for [*M*+H]$^+$.)

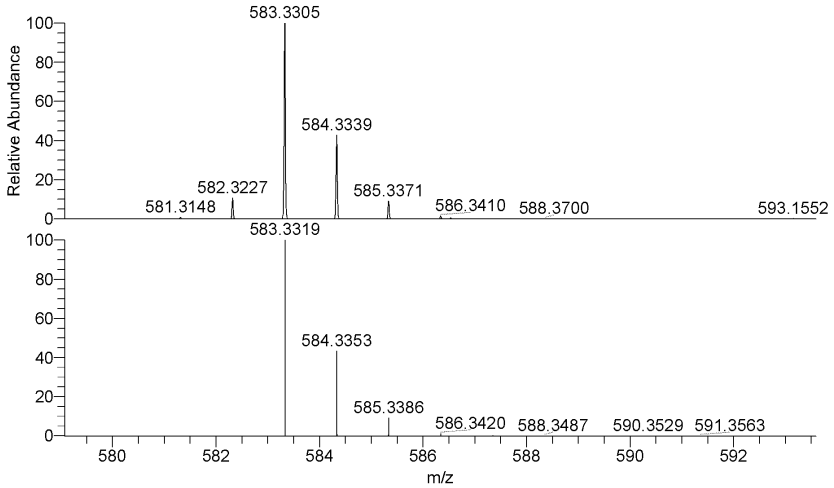

Fig. S4-6 APCI mass spectra of **6-^{t}Bu**. (Top: observed. Bottom: calculated for [*M*+H]$^+$.)

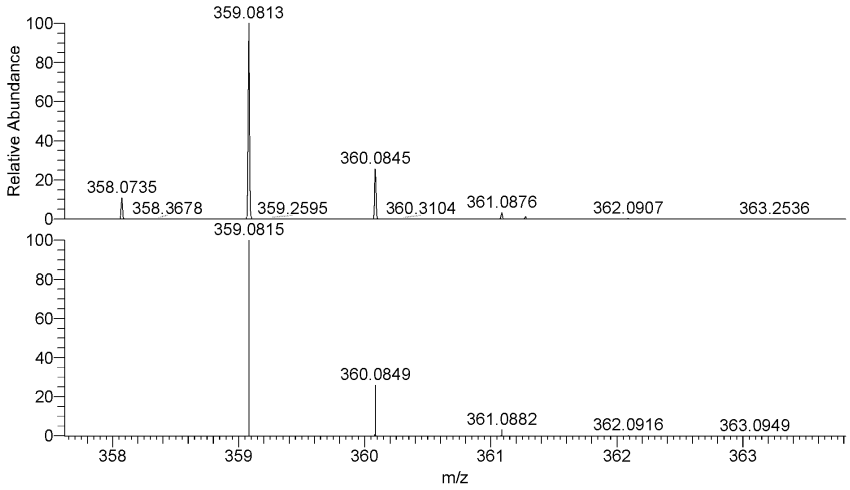

Fig. S4-7 APCI mass spectra of **6**. (Top: observed. Bottom: calculated for [*M*+H]$^+$.)

5. IR Spectra

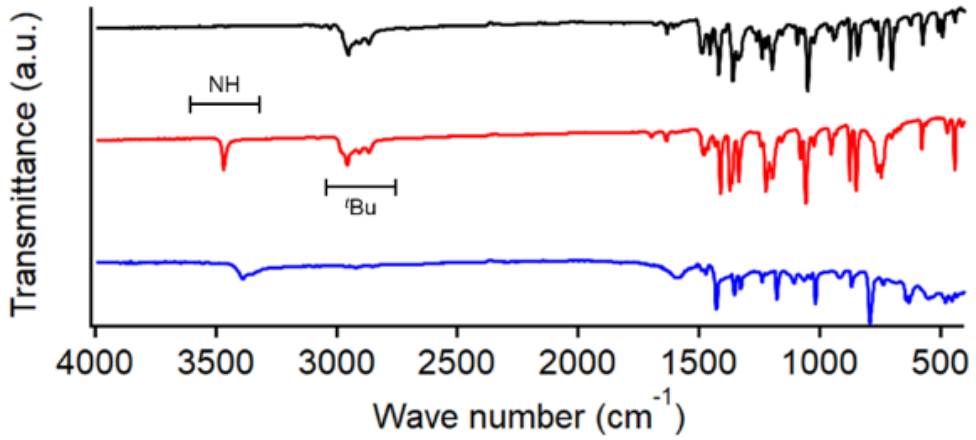

Fig. S5-1 IR spectra of **6-PE-^{t}Bu** (top, black), **6-^{t}Bu** (middle, red) and **6** (bottom, blue).

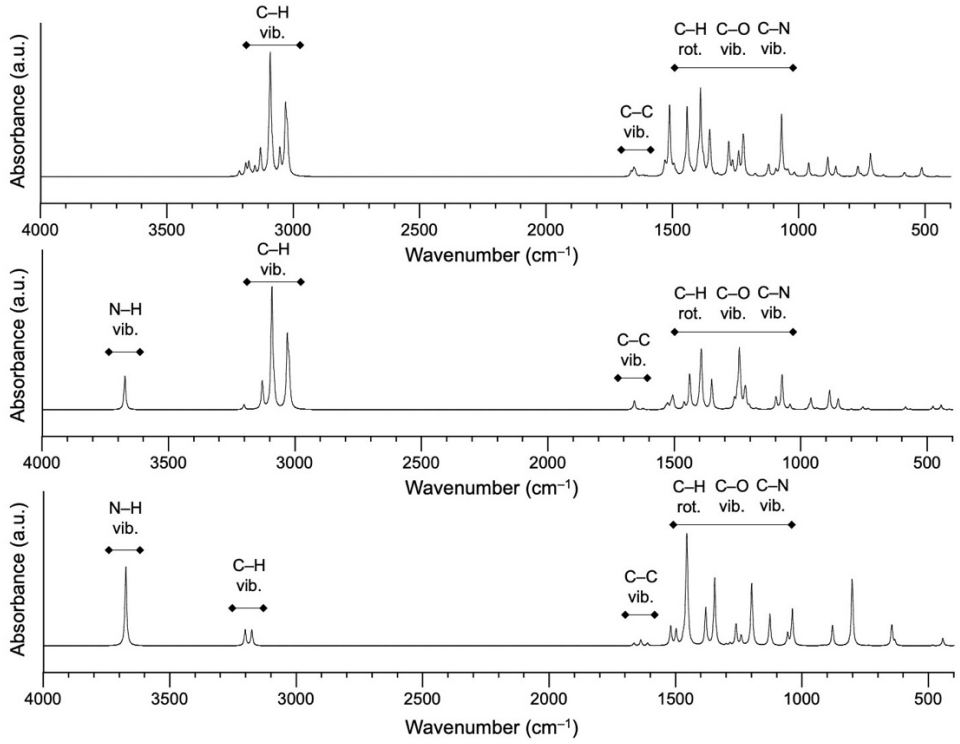

Fig. S5-2 Calculated IR spectra of **6-PE-^{t}Bu** (top), **6-^{t}Bu** (middle) and **6** (bottom) at the level of B3LYP/6-311G(d,p) based on the optimized structures. Half-width-at-half-height was set at 4 cm^{-1}.

6. X-Ray Analysis

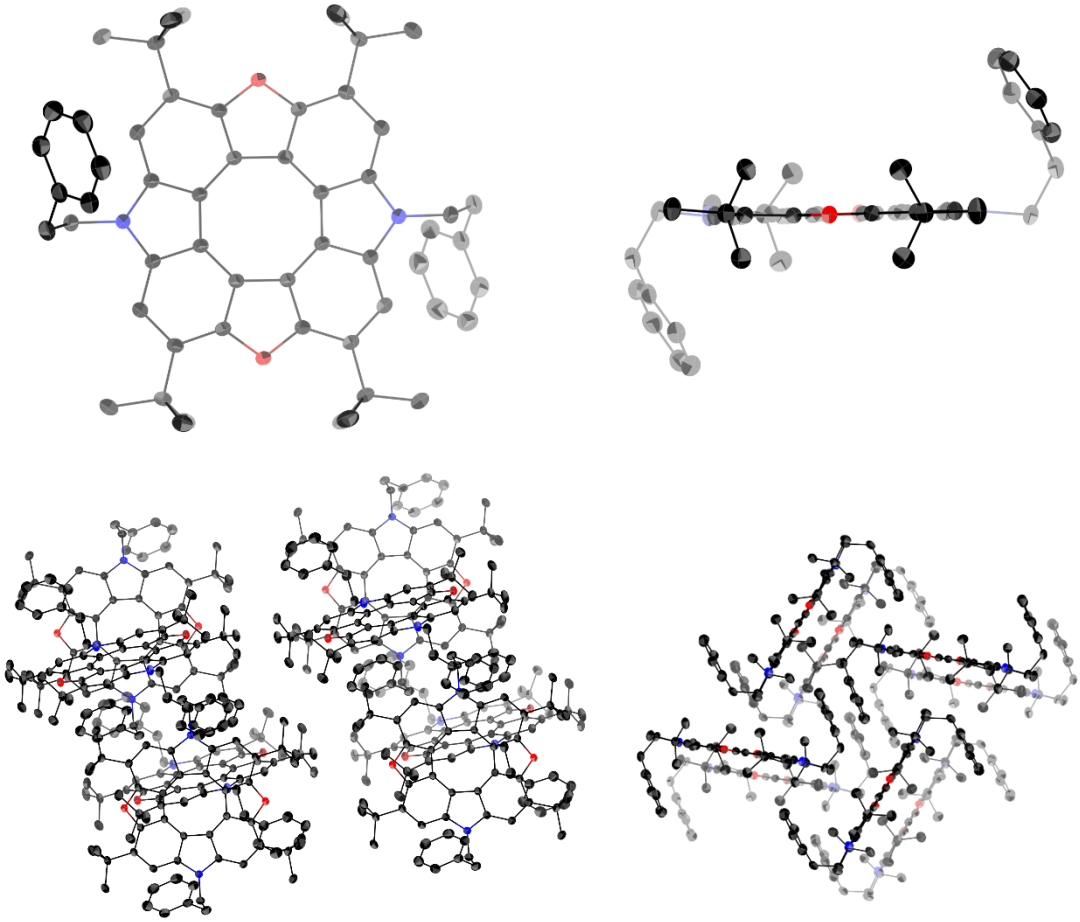

Fig. S6-1 Single crystal X-ray structure for **6-PE-ᵗBu**. The thermal ellipsoids are scaled at 50% probability level. Hydrogen atoms are omitted for clarity.

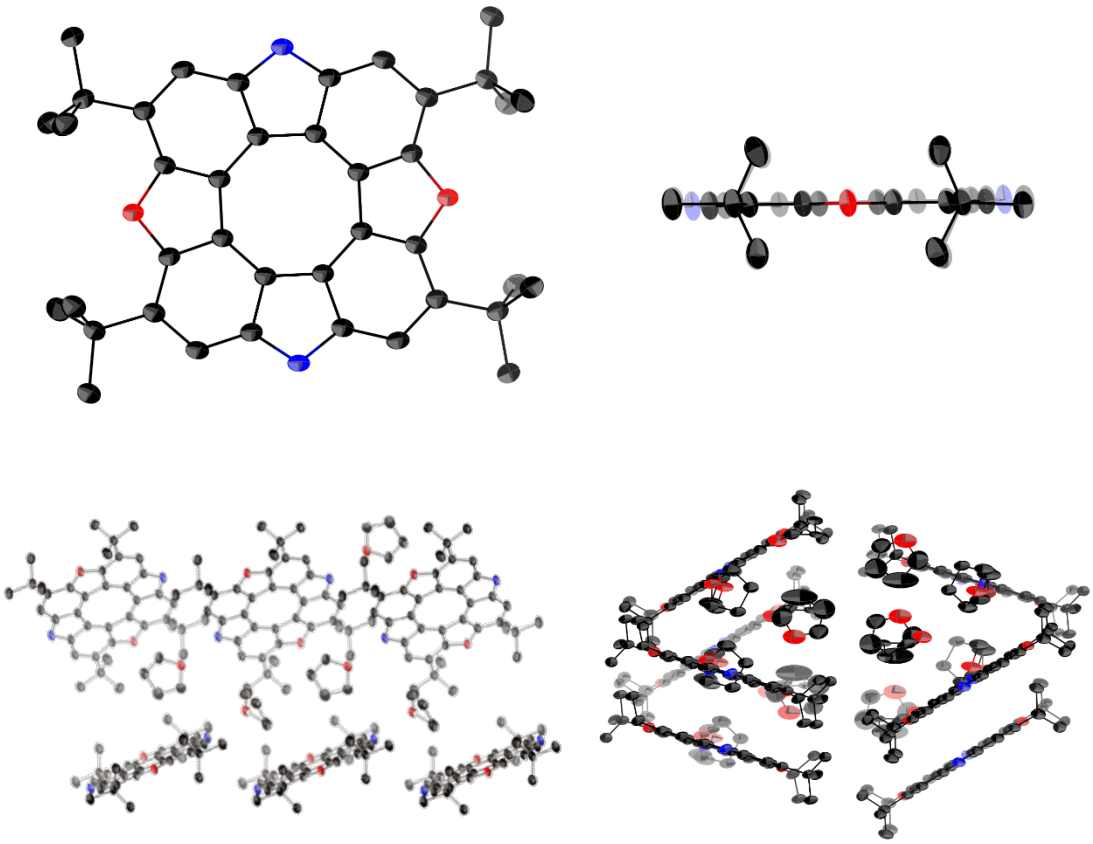

Fig. S6-2 Single crystal X-ray structure for **6-^{t}Bu**. The thermal ellipsoids are scaled at 50% probability level. Hydrogen atoms are omitted for clarity.

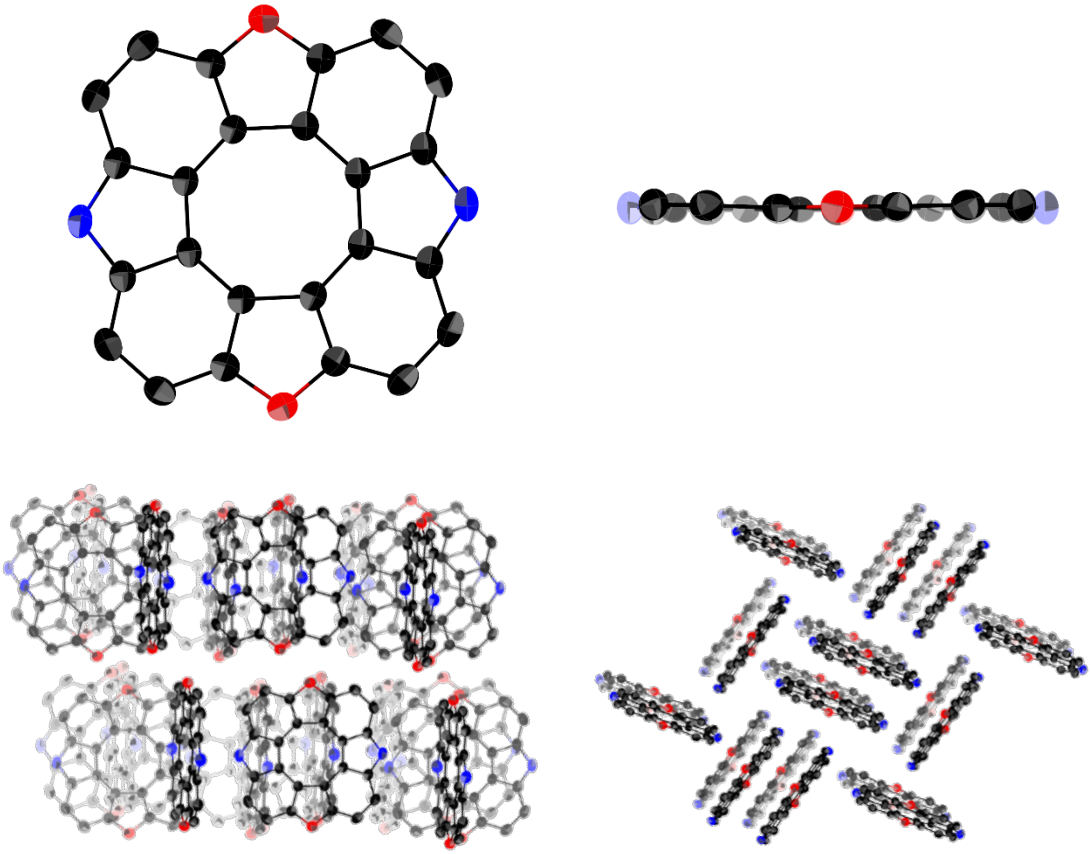

Fig. S6-3 Single crystal X-ray structure for **6**. The thermal ellipsoids are scaled at 50% probability level. Hydrogen atoms are omitted for clarity.

Table S4 Crystal data and structure refinements for **6-PE-^{t}Bu**, **6-^{t}Bu** and **6**.

Compound	**6-PE-^{t}Bu**	**6-^{t}Bu**	**6**
Empirical Formula	$C_{56}H_{58}N_2O_2$	$C_{40}H_{42}N_2O_2 \cdot 4.5(C_4H_8O) \cdot 2.25O$	$C_{24}H_{10}N_2O_2$
M_W	791.04	943.22	358.34
Crystal System	monoclinic	triclinic	monoclinic
Space Group	$P2_1/c$	P-1	$P2_1/c$
a [Å]	11.8608(1)	10.2049(1)	10.0418(4)
b [Å]	13.4284(1)	16.5666(3)	14.1923(4)
c [Å]	27.8740(1)	17.5296(2)	10.9180(3)
α[deg]	90	109.901(2)	90
β[deg]	90.771(1)	90.100(1)	106.166(3)
γ[deg]	90	106.501(2)	90
Volume [Å^3]	4439.13(5)	2655.85(8)	1494.47(9)
Z	4	2	4
Density [g/cm^3]	1.184	1.179	1.593
Completeness	0.988	0.982	0.990
Goodness-of-fit	1.067	1.028	1.069
R_1 [$I > 2\sigma(I)$]	0.0434	0.0773	0.0401
wR_2 (all data)	0.1366	0.2325	0.1143
Solvent System	CH_2Cl_2 / n-hexane	THF / H_2O	THF / n-hexane
CCDC	2346719	2346718	2346717

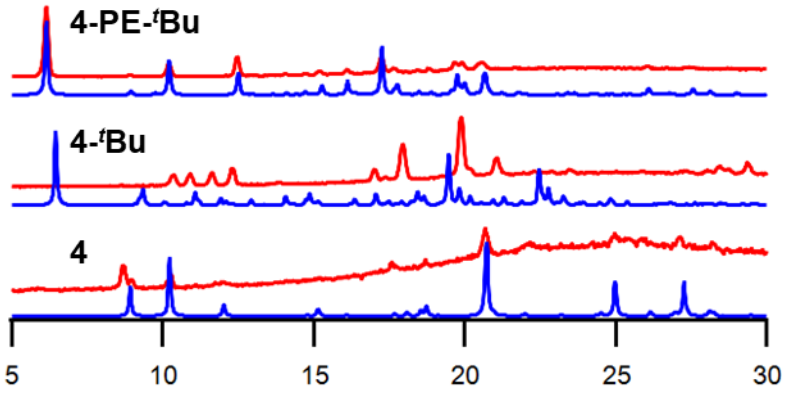

Fig. S6-4 PXRD spectra of **6-PE-^{t}Bu**, **6-^{t}Bu** and **6**. Red lines are measured and blue ones are calculated spectra from single crystal structures.

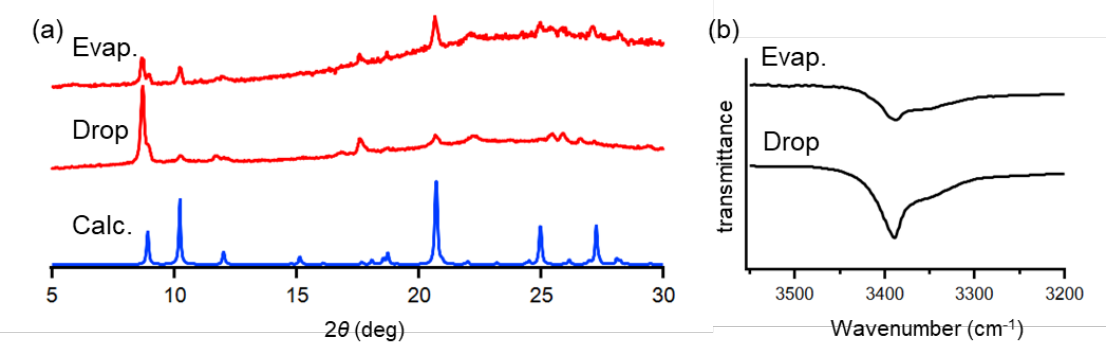

Fig. S6-5 (a) PXRD spectra of **6** in the powder states prepared by two ways; i) evaporation from THF solution (Evap.), and ii) dropping a THF solution into *n*-hexane (Drop). Calculated PXRD spectrum (Calc.) is shown in the bottom. (b) Selected region of the IR spectra of **6**.

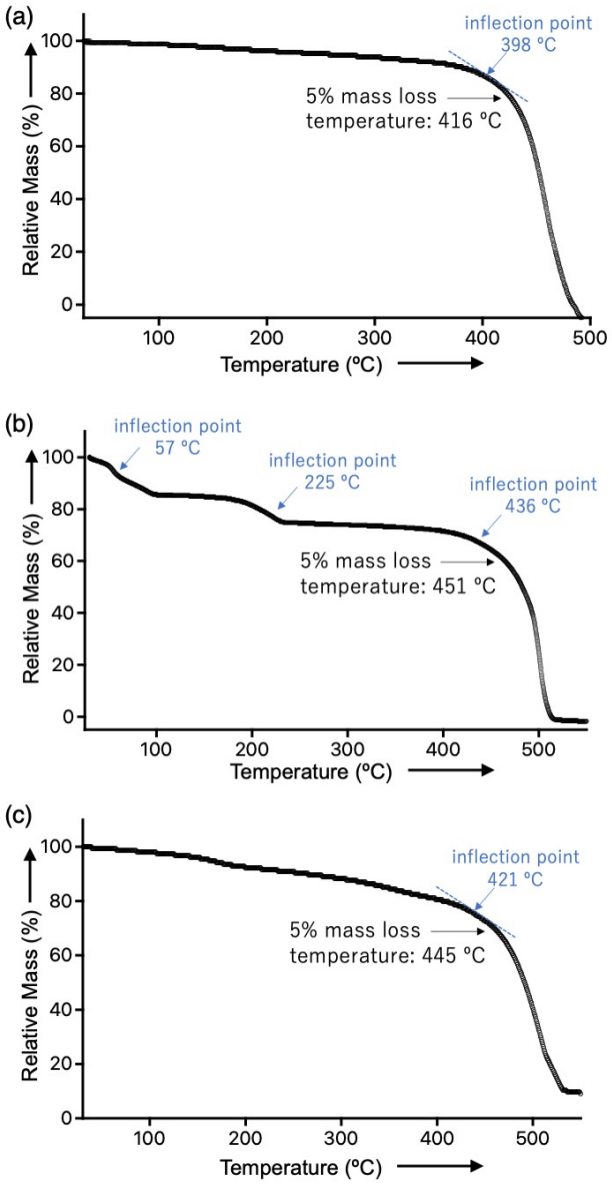

Fig. S6-6 Thermogravimetric analysis (TGA) traces for (a) **6-PE-^{t}Bu**, (b) **6-^{t}Bu** and (c) **6**.

7. Optical Studies

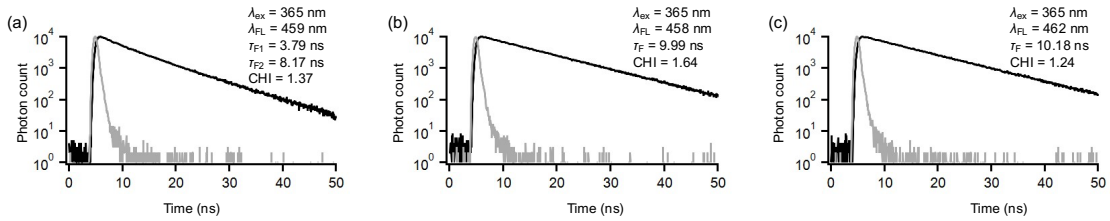

Fig. S7-1 Fluorescence decay profiles for (a) **6-PE-^{t}Bu**, (b) **6-^{t}Bu** and (c) **6** in THF. Gray lines are instrument response function (IRF).

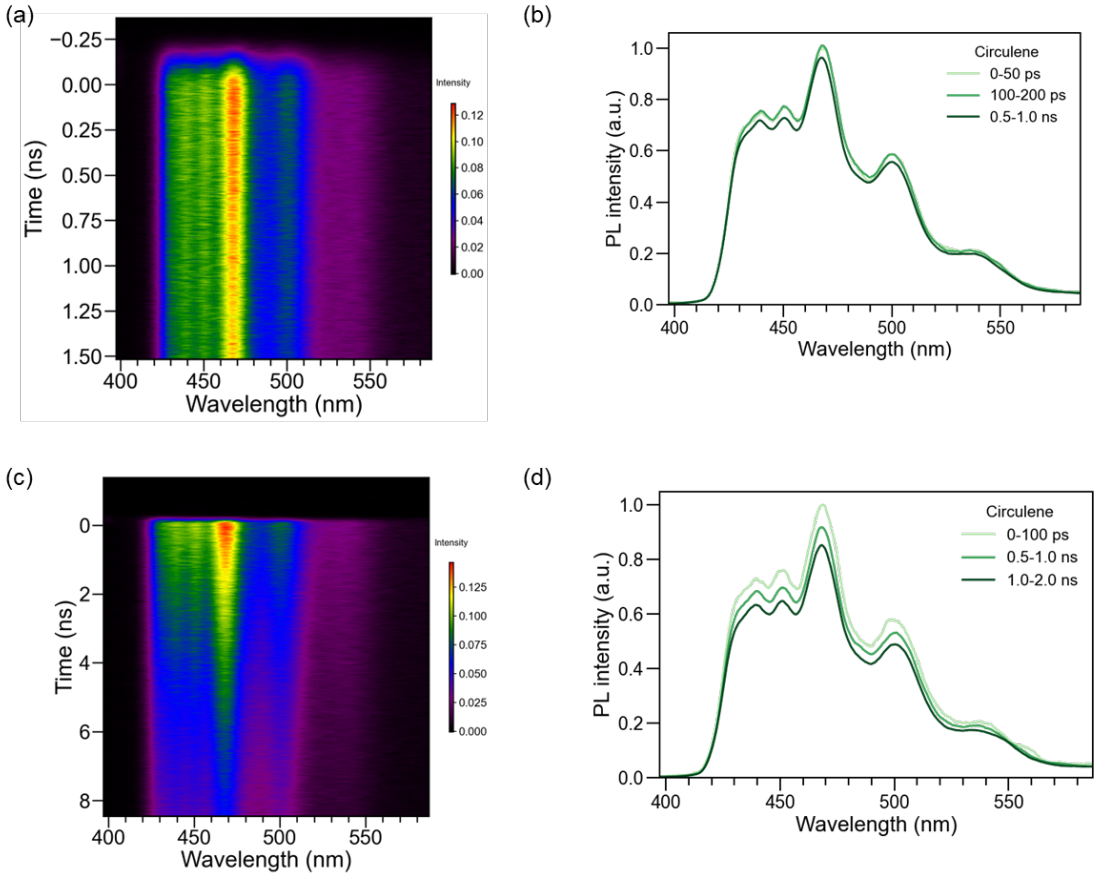

Fig. S7-2 Time-resolved photoluminescence spectroscopy of **6**. a) 2D plot and b) spectra in range of 2 ns. c) 2D plot and d) spectra in range of 10 ns.

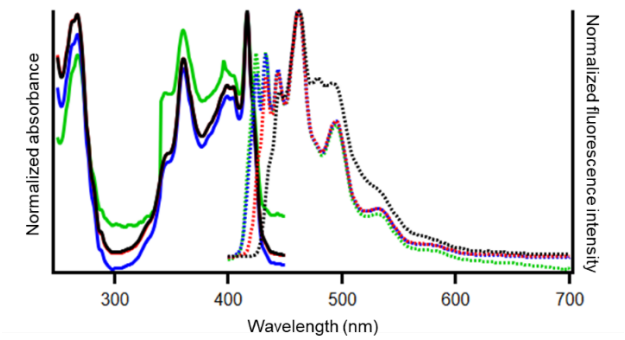

Fig. S7-3 Absorption and fluorescence spectra of **6** in different concentrations ([**6**] = 7.4×10^{-4} M for black line, 7.4×10^{-5} M for red line, 7.4×10^{-6} M for blue line and 7.4×10^{-7} M for green line). λ_{ex} = 380 nm.

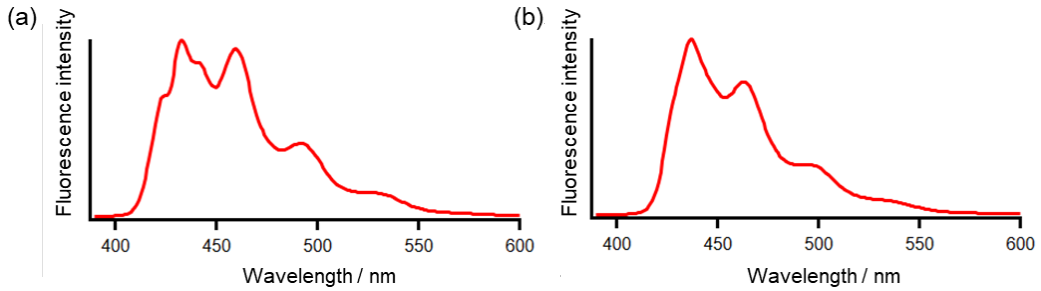

Fig. S7-4 Fluorescence spectra of **6** in (a) acetone and (b) DMSO. [**6**] = 1.1×10^{-5} M for acetone and 1.8×10^{-5} M. λ_{ex} = 380 nm.

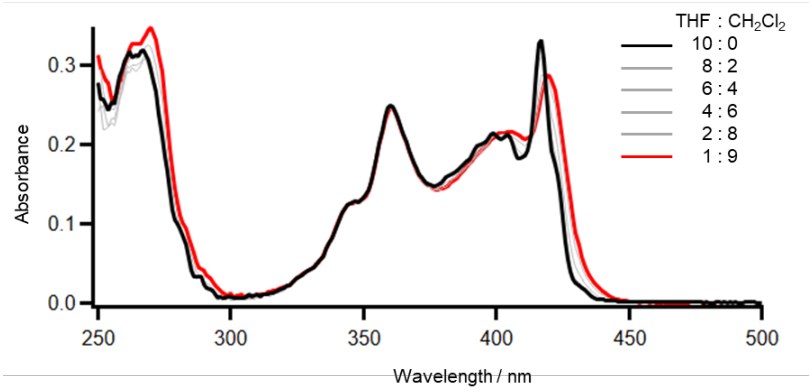

Fig. S7-5 UV/Vis absorption spectra of **6** in a mixture of THF and CH_2Cl_2.

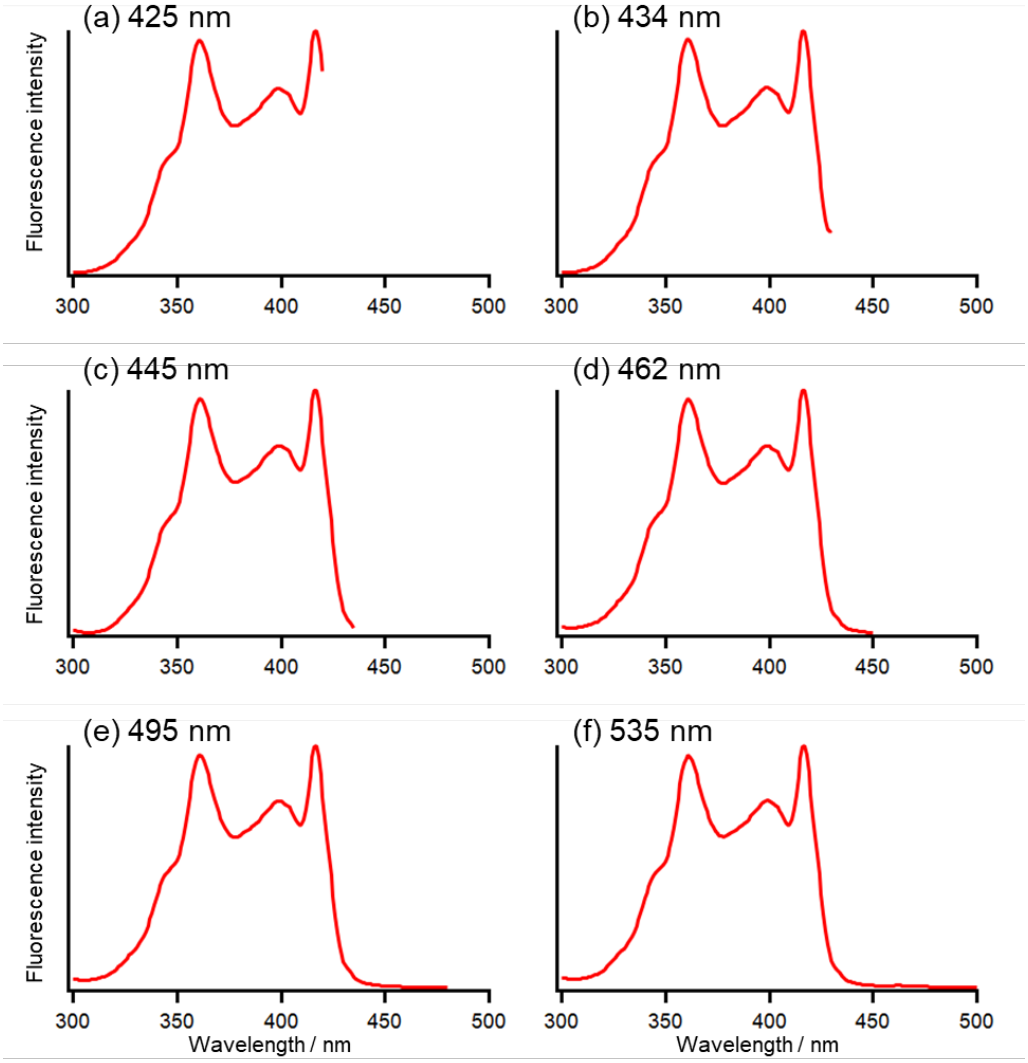

Fig. S7-6 Excitation spectra of **6** in THF at different fluorescence wavelengths.

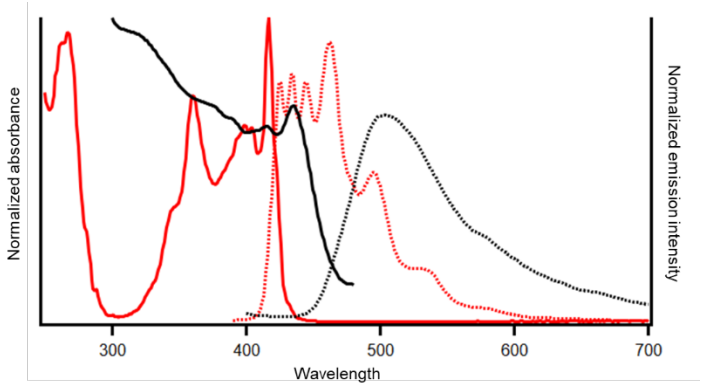

Fig. S7-7 Absorption and emission spectra of **6** in THF (red) and in the solid state (black; prepared by spin coat). Excitation wavelengths: 380 nm.

8. DFT Calculations

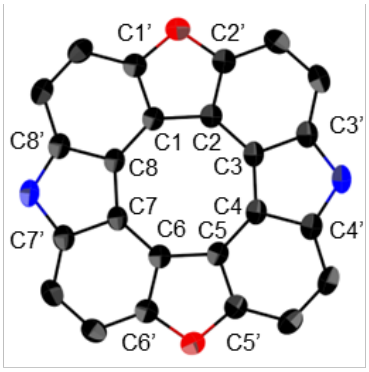

C1-C2: 1.438 Å C1-C1': 1.389 Å
C2-C3: 1.406 Å C2-C2': 1.382 Å
C3-C4: 1.428 Å C3-C3': 1.410 Å
C4-C5: 1.407 Å C4-C4': 1.409 Å
C5-C6: 1.437 Å C5-C5': 1.386 Å
C6-C7: 1.408 Å C6-C6': 1.387 Å
C7-C8: 1.426 Å C7-C7': 1.408 Å
C8-C1: 1.404 Å C8-C8': 1.414 Å

Fig. S8-1 Selected bond lengths of **6** (from crystal structure).

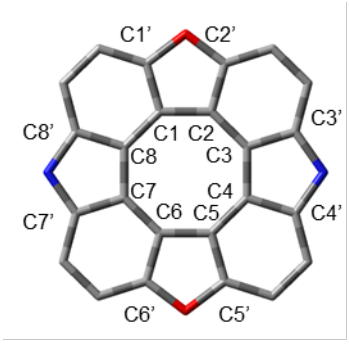

C1-C2: 1.436 Å C1-C1': 1.399 Å
C2-C3: 1.402 Å C2-C2': 1.399 Å
C3-C4: 1.432 Å C3-C3': 1.415 Å
C4-C5: 1.402 Å C4-C4': 1.415 Å
C5-C6: 1.436 Å C5-C5': 1.399 Å
C6-C7: 1.408 Å C6-C6': 1.399 Å
C7-C8: 1.432 Å C7-C7': 1.415 Å
C8-C1: 1.402 Å C8-C8': 1.415 Å

Fig. S8-2 Selected bond lengths of **6** (optimized structure).

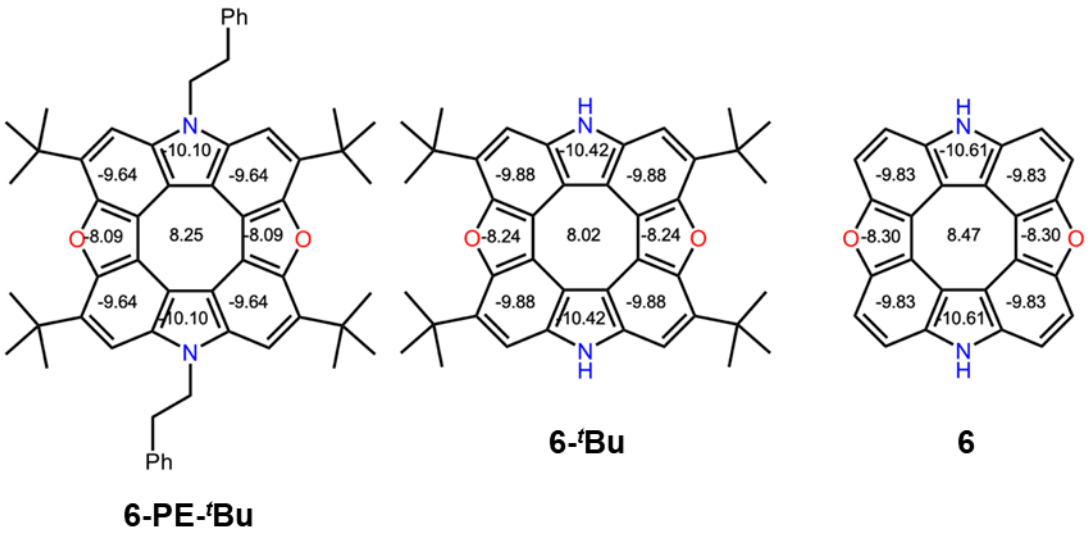

Fig. S8-3 NICS(0) values at the center of each cycles.

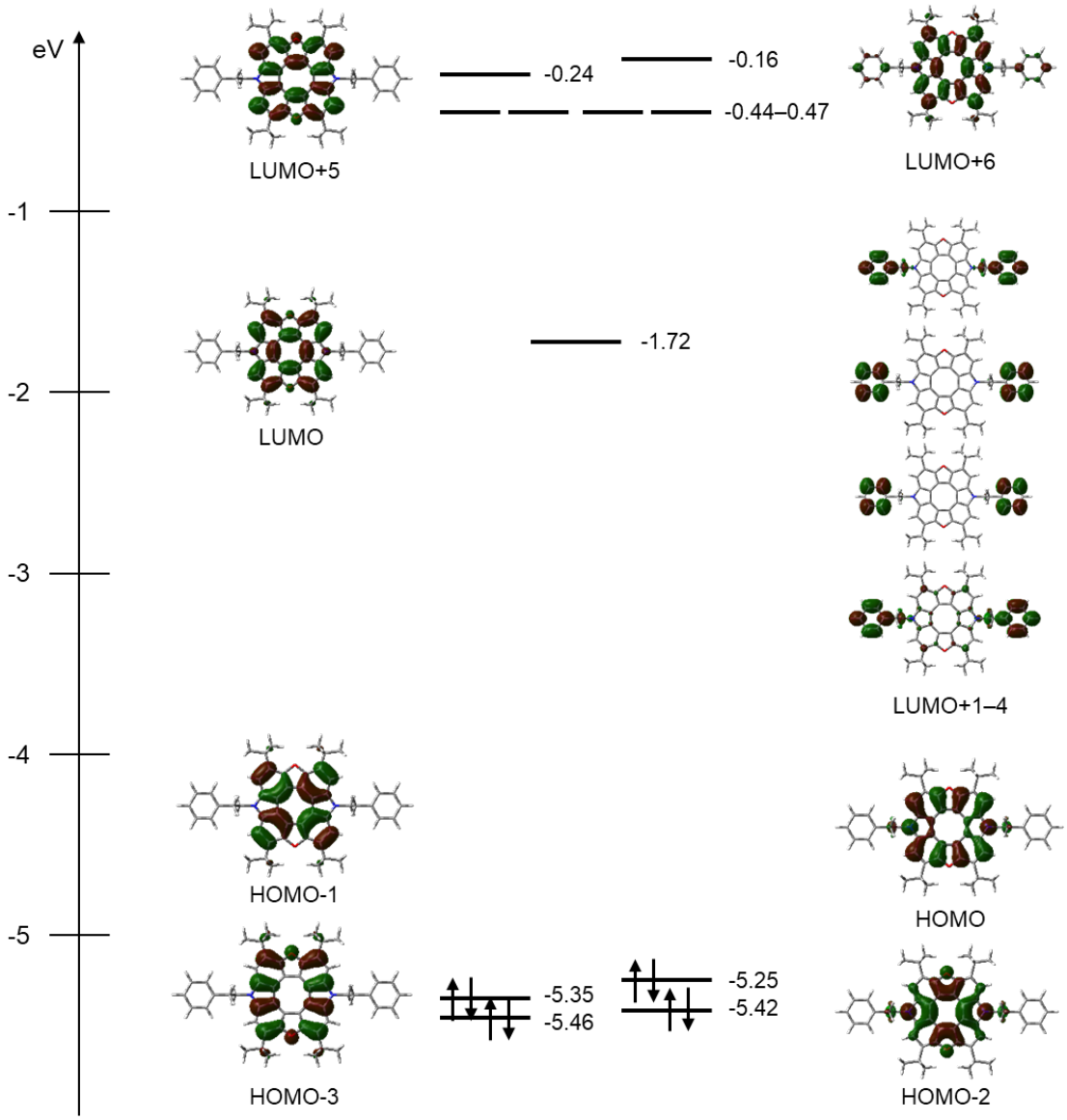

Fig. S8-4 Energy diagram and Kohn-Sham representations for the frontier molecular orbitals of **6-PE-^{t}Bu**.

Table S5 TD-DFT calculated excitation energies and oscillator strengths of **6-^{t}Bu-PE**

Wavelength (nm)	Oscillator strength	Major contributions
418.10	0.0000	H-1 -> LUMO (99 %)
397.97	0.3170	HOMO -> LUMO (97 %)
392.22	0.0000	H-2 -> LUMO (98 %)
370.43	0.3508	H-3 -> LUMO (95 %)
295.46	0.0000	H-4 -> LUMO (89 %) HOMO -> L+5 (7 %)
285.53	0.0028	H-3 -> L+5 (6 %) H-2 -> L+4 (5 %) HOMO -> L+1 (74 %) HOMO -> L+6 (12 %)
282.06	0.1187	H-2 -> L+1 (22 %) HOMO -> L+4 (77 %)
281.40	0.0000	H-2 -> L+3 (14 %) HOMO -> L+2 (84 %)
281.31	0.0009	H-2 -> L+2 (15 %) HOMO -> L+3 (84 %)
276.97	0.0306	H-3 -> L+4 (5 %) H-2 -> L+5 (32 %) H-1 -> L+1 (56 %) H-1 -> L+6 (4 %)
276.83	0.0023	H-3 -> L+5 (16 %) H-2 -> L+4 (16 %) H-1 -> L+7 (3 %) HOMO -> L+1 (12 %) HOMO -> 6 (52 %)
276.52	0.0000	H-3 -> L+2 (17 %) H-3 -> L+6 (9 %) H-1 -> L+4 (14 %) HOMO -> L+4 (55 %)

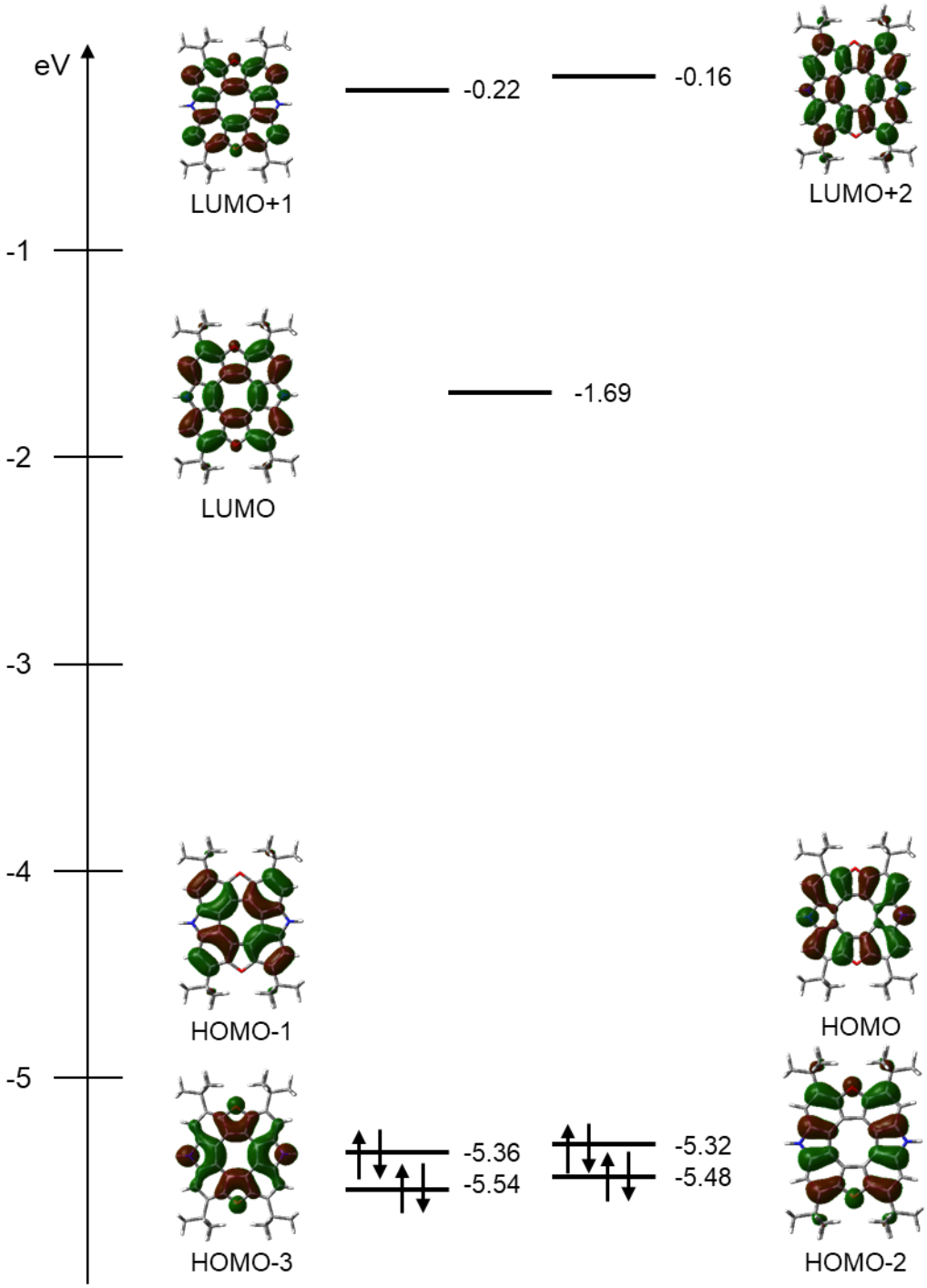

Fig. S8-5 Energy diagram and Kohn-Sham representations for the frontier molecular orbitals of **6-^{t}Bu**.

Table S6 TD-DFT calculated excitation energies and oscillator strengths of **6-^{t}Bu**

Wavelength (nm)	Oscillator strength	Major contributions
412.91	0.0000	H-1 -> LUMO (99 %)
384.12	0.2235	H-1 -> L+1 (2 %) HOMO -> LUMO (96 %)
374.91	0.0000	H-3 -> LUMO (98 %)
365.23	0.4022	H-2 -> LUMO (95 %) H-1 -> L+2 (3 %)
292.06	0.0000	H-4 -> LUMO (90 %) HOMO -> L+1 (6 %)
276.43	0.0000	H-2 -> L+1 (30 %) H-1 -> L+3 (6 %) HOMO -> L+2 (63 %)
270.38	0.0000	H-4 -> LUMO (2 %) H-2 -> L+2 (25 %) HOMO -> L+1 (70 %)
267.11	0.0284	H-3-> L+1 (71 %) H-1 -> L+2 (26 %)
266.36	0.2209	H-6 -> LUMO (3 %) H-3 -> L+2 (8 %) H-1 -> L+1 (84 %)
260.18	0.4119	H-3 -> L+1 (25 %) H-1 -> L+2 (59 %) HOMO -> L+3 (13 %)
260.02	0.0366	H-3 -> L+2 (87 %) H-2 -> L+3 (3 %) H-1 -> L+1 (6 %)
258.20	0.0000	H-5 -> LUMO (2 %) H-2 -> L+1 (63 %) HOMO -> L+2 (30 %)
251.62	0.0000	H-2 -> L+2 (65 %) H-1 -> L+4 (13 %) HOMO -> L+1 (17 %)

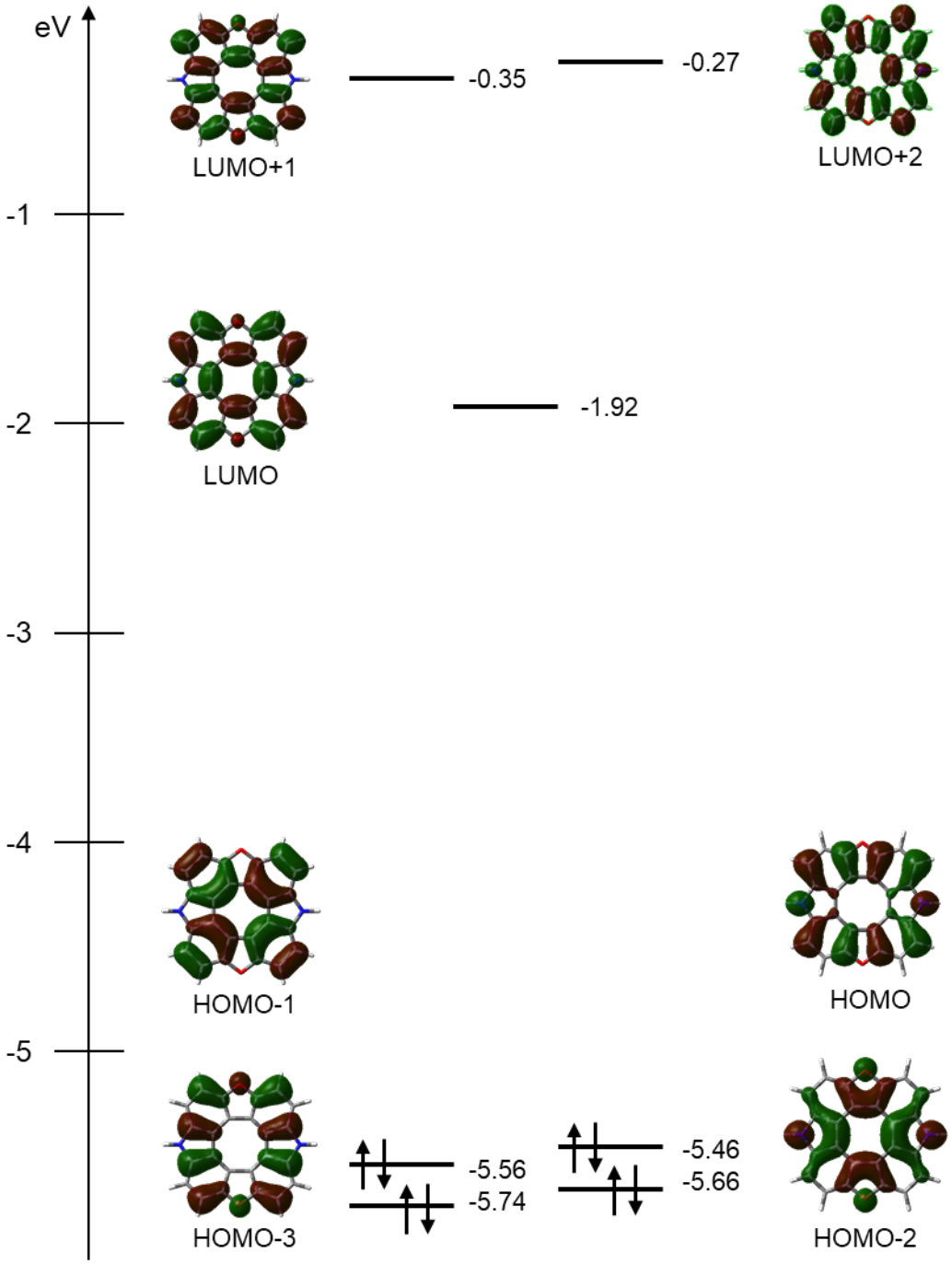

Fig. S8-6 Energy diagram and Kohn-Sham representations for the frontier molecular orbitals of **6**.

Table S7 TD-DFT calculated excitation energies and oscillator strengths of **6**

Wavelength (nm)	Oscillator strength	Major contributions
419.87	0.0000	H-1 -> LUMO (100 %)
390.33	0.2441	H-1 -> L+1 (2 %) HOMO -> LUMO (96 %)
387.10	0.0000	H-2 -> LUMO (98 %)
360.00	0.2310	H-3 -> LUMO (94 %) H-1 -> L+2 (3 %)
290.69	0.0000	H-4 -> LUMO (87 %) HOMO -> L+1 (9 %)
272.79	0.0000	H-3 -> L+1 (19 %) H-1 -> L+3 (7 %) HOMO -> L+2 (74 %)
267.94	0.0000	H-4 -> LUMO (4 %) H-3 -> L+2 (20 %) HOMO -> L+1 (73 %)
266.24	0.001	H-2-> L+1 (89 %) H-1 -> L+2 (9 %)
261.84	0.1608	H-5 -> LUMO (3 %) H-2 -> L+2 (28 %) H-1 -> L+1 (64 %)
259.73	0.1060	H-5 -> LUMO (3 %) H-3 -> L+3 (3 %) H-2 -> L+2 (68 %) H-1 -> L+1 (24 %)
257.23	0.1806	H-7 -> LUMO (2 %) H-2 -> L+1 (8 %) H-1 -> L+2 (73 %) HOMO -> L+3 (14 %)
253.56	0.0000	H-3 -> L+1 (73 %) HOMO -> L+2 (19 %)
244.36	0.0000	H-3 -> L+2 (66 %) H-2 -> L+3 (3 %) H-1 -> L+4 (15 %) HOMO -> L+1 (11 %)

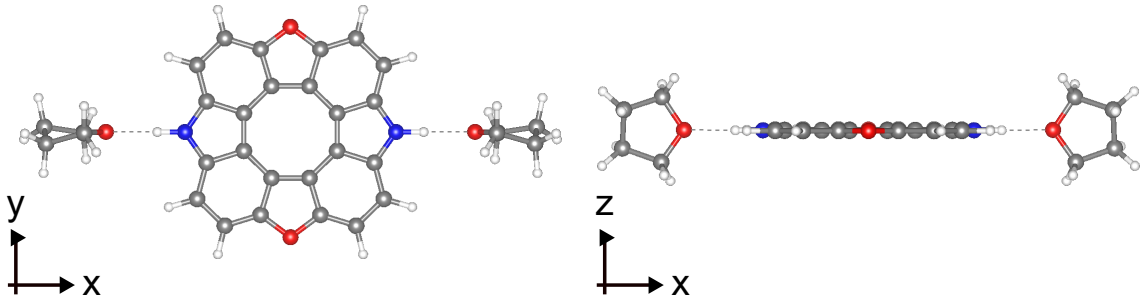

Fig. S8-7 Geometry optimized structure of S_1 state for **6** with THF.

9. Herzberg-Teller Effect

Within the first-order approximation, the fluorescence intensity is proportional to the square of the transition dipole moment between the initial and final electronic states at the equilibrium nuclear configuration. However, even if the transition dipole moment between the initial and final electronic states vanishes (symmetry-forbidden), a molecule can exhibit weak fluorescence because of the symmetry breaking by molecular vibration. This is called the Herzberg-Teller effect,[S11] and the theory is briefly described below.

We consider a molecule that consists of M nuclei and N electrons. A set of electronic coordinates is denoted by $\mathbf{r} = (\mathbf{r}_1, \cdots, \mathbf{r}_i, \cdots \mathbf{r}_N)$, where $\mathbf{r}_i = (x_i, y_i, z_i)$ in the Cartesian coordinates, and a set of mass-weighted normal coordinates is denoted by $\mathbf{Q} = (Q_1, \cdots, Q_\alpha, \cdots Q_{3M-5 \text{ or } 3M-6})$. The vibronic Hamiltonian is given by

$$\mathcal{H}(\mathbf{r}, \mathbf{Q}) = \mathcal{T}_N(\mathbf{Q}) + \mathcal{H}_e(\mathbf{r}, \mathbf{Q}), \tag{S1}$$

where $\mathcal{T}_N(\mathbf{Q})$ is the nuclear kinetic energy operator and $\mathcal{H}_e(\mathbf{r}, \mathbf{Q})$ is the electronic Hamiltonian. The electronic Schrödinger equation is given by

$$[\mathcal{H}_e(\mathbf{r}, \mathbf{Q}) - E_m(\mathbf{Q})]\Psi_m(\mathbf{r}, \mathbf{Q}) = 0, \tag{S2}$$

where $E_m(\mathbf{Q})$ is the electronic energy and $\Psi_m(\mathbf{r}, \mathbf{Q})$ is the electronic wavefunction. Within the Born-Oppenheimer approximation, the vibronic wave function $\Phi_{mv}(\mathbf{r}, \mathbf{Q})$ is expressed as a product of the electronic and vibrational wavefunctions $\chi_{mv}(\mathbf{Q})$,[S12]

$$\Phi_{mv}(\mathbf{r}, \mathbf{Q}) = \Psi_m(\mathbf{r}, \mathbf{Q})\chi_{mv}(\mathbf{Q}), \tag{S3}$$

where $v = (v_1, \cdots, v_\alpha, \cdots, v_{3M-5 \text{ or } 3M-6})$ is a set of vibrational quantum numbers. The vibrational Schrödinger equation is given by

$$[\mathcal{T}_N(\mathbf{Q}) + E_m(\mathbf{Q}) - E_{mv}]\chi_{mv}(\mathbf{Q}) = 0, \tag{S4}$$

where E_{mv} is the vibronic energy.

The Herzberg-Teller expansion of $\mathcal{H}_e(\mathbf{r}, \mathbf{Q})$ around the reference nuclear configuration $\mathbf{Q} = \mathbf{0}$ (in this study, the reference nuclear configuration was taken at the equilibrium geometry of S_1, i.e., the initial electronic state of fluorescence) is given by[S11]

$$\mathcal{H}_e(\mathbf{r}, \mathbf{Q}) = \mathcal{H}_e(\mathbf{r}, \mathbf{0}) + \sum_\alpha \left(\frac{\partial \mathcal{H}_e(\mathbf{r}, \mathbf{Q})}{\partial Q_\alpha}\right)_\mathbf{0} Q_\alpha + \cdots. \tag{S5}$$

The electronic Schrödinger equation for $\mathcal{H}_e(\mathbf{r}, \mathbf{0})$ is given by

$$[\mathcal{H}_e(\mathbf{r}, \mathbf{Q}) - E_m(\mathbf{0})]\Psi_m(\mathbf{r}, \mathbf{0}) = 0, \tag{S6}$$

where $E_m(\mathbf{0})$ and $\Psi_m(\mathbf{r}, \mathbf{0})$ are the electronic energy and wavefunction clamped at $\mathbf{Q} = \mathbf{0}$. Based on the Rayleigh-Schrödinger perturbation theory, $\Psi_m(\mathbf{r}, \mathbf{Q})$ can be expressed using $\Psi_m(\mathbf{r}, \mathbf{0})$ as follows:[S12]

$$\Psi_m(\mathbf{r}, \mathbf{Q}) = \Psi_m(\mathbf{r}, \mathbf{0}) + \sum_{k \neq m} \frac{\sum_\alpha V_{km,\alpha} Q_\alpha}{E_m(\mathbf{0}) - E_k(\mathbf{0})} \Psi_k(\mathbf{r}, \mathbf{0}) + \cdots, \tag{S7}$$

where $V_{km,\alpha}$ is the vibronic coupling constant defined by

$$V_{km,\alpha} = \left\langle \Psi_k(\mathbf{r},\mathbf{0}) \middle| \left(\frac{\partial \mathcal{H}_e(\mathbf{r},\mathbf{Q})}{\partial Q_\alpha}\right)_{\mathbf{0}} \middle| \Psi_m(\mathbf{r},\mathbf{0}) \right\rangle. \tag{S8}$$

We consider the transition from initial electronic state m to final state n. The transition dipole moment between electronic states m and n is given by

$$\mu_{nm}(\mathbf{Q}) = \langle \Psi_n(\mathbf{r},\mathbf{Q}) | \hat{\mu}(\mathbf{r}) | \Psi_m(\mathbf{r},\mathbf{Q}) \rangle, \tag{S9}$$

where $\hat{\mu}(\mathbf{r})$ is the electric dipole moment operator defined by

$$\hat{\mu}(\mathbf{r}) = -\sum_i e\mathbf{r}_i, \tag{S10}$$

with e being the elementary charge. Substituting Eq. (S7) into Eq (S9), the transition dipole moment is written as

$$\mu_{nm}(\mathbf{Q}) = \mu_{nm}(\mathbf{0}) + \sum_\alpha \left[\sum_{k\neq m} \frac{\mu_{nk}(\mathbf{0}) V_{km,\alpha}}{E_m(\mathbf{0}) - E_k(\mathbf{0})} + \sum_{\ell \neq n} \frac{V^*_{\ell n,\alpha} \mu_{\ell m}(\mathbf{0})}{E_n(\mathbf{0}) - E_\ell(\mathbf{0})} \right] Q_\alpha + \cdots. \tag{S11}$$

We consider the case where $\mu_{nm}(\mathbf{0}) = 0$ (symmetry-forbidden). Also, we consider the fluorescence from S_1 to S_0. In this case, the intermediate electronic states k and ℓ are energetically higher enough than S_1, which indicates $|E_m(\mathbf{0}) - E_k(\mathbf{0})| \ll |E_n(\mathbf{0}) - E_\ell(\mathbf{0})|$. Therefore, only the first term in the square bracket on the right-hand equation was considered below. The fluorescence occurs by borrowing the non-zero translon dipole moment between electronic states k and n. Based on the Fermi's golden rule, the fluorescence spectrum from electronic state m to n is given by[S13]

$$\sigma(\omega) = \frac{\omega^3}{3\pi c^3 \varepsilon_0} \left| \sum_{k\neq m} \sum_\alpha \frac{\mu_{nk}(\mathbf{0}) V_{km,\alpha}}{E_m(\mathbf{0}) - E_k(\mathbf{0})} \right|^2 |\langle \chi_{n\nu'} | Q_\alpha | \chi_{m\nu} \rangle|^2 \delta(E_{n\nu'} - E_{m\nu} + \hbar\omega), \tag{S12}$$

where ω and c are the frequency and speed of photon, respectively, and ε_0 is the vacuum permittivity. The vibrational part of the fluorescence spectrum was evaluated by approximating the vibrational wavefunction to the eigenfunction of the displaced harmonic oscillator (see Ref. [S14] for details). The 0-0 transition does not appear in the Herzberg-Teller spectrum because of Q_α in the vibrational matrix element.

In Eq. (S12), the density of the final vibronic states was expressed using the delta function. In this study, the broadening of the density of final vibronic states, which arises from the interactions with the surrounding environment, was expressed using the Gaussian function,

$$\sigma(\omega) = \frac{\omega^3}{3\pi c^3 \varepsilon_0} \left| \sum_{k\neq m} \sum_\alpha \frac{\mu_{nk}(\mathbf{0}) V_{km,\alpha}}{E_m(\mathbf{0}) - E_k(\mathbf{0})} \right|^2 |\langle \chi_{n\nu'} | Q_\alpha | \chi_{m\nu} \rangle|^2 \frac{1}{\sqrt{2\pi\sigma^2}} e^{-\frac{\left(E_{n\nu'} - (E_{m\nu} - \hbar\omega)\right)^2}{2\sigma^2}}. \tag{S13}$$

Here, σ is the linewidth of the Gaussian function, which was determined so as to reproduce the linewidth of the experimental fluorescence spectrum.

10. Supporting References

S1 a) G. M. Sheldrick, *Acta Cryst. A*, 2008, **64**, 112. b) G. M. Sheldrick, *Acta Cryst. C*, 2015, **71**, 3.

S2 Gaussian 16, Revision C.01, M. J. Frisch, G. W. Trucks, H. B. Schlegel, G. E. Scuseria, M. A. Robb, J. R. Cheeseman, G. Scalmani, V. Barone, G. A. Petersson, H. Nakatsuji, X. Li, M. Caricato, A. V. Marenich, J. Bloino, B. G. Janesko, R. Gomperts, B. Mennucci, H. P. Hratchian, J. V. Ortiz, A. F. Izmaylov, J. L. Sonnenberg, D. Williams-Young, F. Ding, F. Lipparini, F. Egidi, J. Goings, B. Peng, A. Petrone, T. Henderson, D. Ranasinghe, V. G. Zakrzewski, J. Gao, N. Rega, G. Zheng, W. Liang, M. Hada, M. Ehara, K. Toyota, R. Fukuda, J. Hasegawa, M. Ishida, T. Nakajima, Y. Honda, O. Kitao, H. Nakai, T. Vreven, K. Throssell, J. A. Montgomery, Jr., J. E. Peralta, F. Ogliaro, M. J. Bearpark, J. J. Heyd, E. N. Brothers, K. N. Kudin, V. N. Staroverov, T. A. Keith, R. Kobayashi, J. Normand, K. Raghavachari, A. P. Rendell, J. C. Burant, S. S. Iyengar, J. Tomasi, M. Cossi, J. M. Millam, M. Klene, C. Adamo, R. Cammi, J. W. Ochterski, R. L. Martin, K. Morokuma, O. Farkas, J. B. Foresman and D. J. Fox, Gaussian, Inc., Wallingford CT, 2016.

S3 a) A. D. Becke, *J. Chem. Phys.*, 1993, **98**, 1372. b) C. Lee, W. Yang and R. G. Parr, *Phys. Rev. B*, 1988, **37**, 785.

S4 H. F. B. Shaidaei, C. S. Wannere, C. Corminboeuf, R. Puchta, P. v. R. Schleyer, *Org. Lett*., 2006, **8**, 863.

S5 a) B. Xu, E. Sheibani, P. Liu, J. Zhang, H. Tian, N. Vlachopoulos, G. Boschloo, L. Kloo, A. Hagfeldt and L. Sun, *Adv. Mater.*, 2014, **26**, 6629. b) A. Rembiak and A. M. P. Koskinen, *Synthesis*, 2015, **47**, 3347.

S6 F. Chen, Y. S. Hong, S. Shimizu, D. Kim, T. Tanaka and A. Osuka, *Angew. Chem., Int. Ed.,* 2015, **54**, 10639.

S7 Y. Matsuo, F. Chen, K. Kise, T. Tanaka and A. Osuka, *Chem. Sci.*, 2019, **10**, 11006.

S8 Y. Matsuo, T. Tanaka and A. Osuka, *Chem. Eur. J.*, 2020, **26**, 8144.

S9 B. Lousen, S. K. Pedersen, P. Bols, K. H. Hansen, M. R. Pedersen, O. Hammerich, S. Bondarchuk, B. Minaev, G. V. Baryshnikov, H. Ågren and M. Pittelkow, *Chem. Eur. J.*, 2020, **26**, 4935.

S10 T. Hensel, D. Trpcevski, C. Lind, R. Grosjean, P. Hammershøj, C. B. Nielsen, T. Brock-Nannestad, B. E. Nielsen, M. Schau-Magnussen, B. Minaev, G. V. Baryshnikov and M. Pittelkow, *Chem. Eur. J.*, 2013, **19**, 17097.

S11 G. Herzberg and E. Teller, *Z. Physik. Chem. (Leipzig*), 1933, **B21**, 410.

S12 a) T. Azumi and K. Matsuzaki, *Photochem. Photobiol.*, 1977, **25**, 315. b) G. Fischer, *Vibronic Coupling: The Interaction between the Electronic and Nuclear Motions,* Academic Press, London, 1984.

S13 a) J. J. Sakurai, *Advanced Quantum Mechanics*, Addison-Wesley, Reading, MA, 1967. (b) D. P. Craig and T. Thirunamachandran, *Molecular Quantum Electrodynamics: An Introduction to Radiation-Molecular Interactions,* Dover, New York, 1998.

S14 a) W. Ota, M. Uejima and T. Sato, *Bull. Chem. Soc. Jpn.*, 2023, **96**, 582. b) W. Ota, M. Uejima, N. Haruta and T. Sato, *Bull. Chem. Soc. Jpn.*, 2024, **97**, uoad020.